Modeling Electrical Conductivity for Earth Media with Macroscopic Fluid-Filled Fractures

James G. Berryman[1] and G. Michael Hoversten[2]

[1]*Lawrence Berkeley National Laboratory,*

One Cyclotron Road MS 90R1116, Berkeley,

CA 94740, USA, E-mail: jgberryman@lbl.gov

[2]*Chevron Energy Technology Co., 6001 Bollinger Canyon Road,*

San Ramon, CA 94583, E-mail: HOVG@chevron.com

Abstract

Effective medium theories for either highly conductive or more resistive electrical inclusions in a moderately conducting background medium are presented for modeling macroscopic (*i.e.*, large-scale) fluid-filled fractures or cracks in a potential reservoir rock or granular medium. Conductive fluids are most often brine and resistive fluids of interest are oil, gas, air, and/or CO_2. Novel features of the presentation for conductive fluids include results for both non-interacting inclusions (using a Maxwell approximation), and for interacting inclusions (via a self-consistent effective medium scheme). The anisotropic analysis is specifically designed to handle reservoirs with multiple orientations (usually three orthogonal sets) of oblate spheroidal cracks/fractures, while also having arbitrary aspect ratios. But these aspect ratios are strictly < 1, thus excluding spherical pores and simple granular media – both already been widely studied by others. Results show that the self-consistent approximation depends on fracture aspect ratio α and this approximation becomes important when fracture porosity is about $\phi = 1\%$ for aspect ratio $\alpha \simeq 0.05$, or $\phi = 3\%$ for aspect ratio $\alpha \simeq 0.10$. It is shown that the self-consistent analysis is most important when the fractures have very small aspect ratio — the inferred reason being that the fracture (or crack) number density ($\rho_c \equiv \phi/\alpha$) then becomes very high and the fracture relative spacing correspondingly very small for any fixed value of porosity (but with decreasing values of aspect ratio). Hybrid methods (combining self-consistent and non-self-consistent formulas) are also developed to deal with high volume fractions and multiple sets of fractures having different aspect ratios. Whenever possible and appropriate, the results are also compared to rigorous bounds, including the Wiener bounds and the Hashin-Shtrikman bounds, in order to provide one type of partial validation of the methods being developed.

INTRODUCTION

In many (perhaps most) electrical/electromagnetic surveys of earth media, the modeling aspect of the problem is generic, by which we mean to say that no specific microstructure is assumed to be present. Rather, electrical/electromagnetic modeling is limited to using either finite element or finite difference modeling approaches that make no special assumptions about the micro-scale causes of the conductivity used either at grid points, or within finite element cells (Dey & Morrison, 1979; LaBrecque *et al.*, 1996; Zhou & Greenhalgh, 2001; Hoversten *et al.*, 2006a,b; Zhou *et al.*, 2009; Newman *et al.*, 2010).

There is currently no adequate theory to provide the needed link between micro-scale (*i.e.*, below the scale of typically used finite difference or finite element cells $\simeq$ 100m), macroscopic fracturing, and the effective electrical conductivity at a scale appropriate for this modeling. **There has been considerable effort expended on the somewhat similar problem of fluid permeability or hydraulic conductivity (Berryman, 1985; Berryman and Milton, 1985). However, there are good reasons not to use this analogy here. First, there is the very important qualitative difference between fluid permeability and electrical conductivity which is that the pertinent macroscopic equation for permeability (*i.e.*, Darcy's law) does not have the same form as the underlying fundamental equation (which is the Navier-Stokes equation), whereas the equations for microscopic electrical conduction and macroscopic electrical conduction take the same form. Also, because of the well-known scale invariance of electrical conductivity, and the equally well-known lack of scale invariance for hydraulic conductivity — see Whitherspoon et al. (1980), Long et al. (1982), Renard and de Marsily (1997), and Fokker (2001) — this analogy, although useful if it were appropriate, will unfortunately not be available to us here.** The lack of such a general theory of electrical conduction in macroscopic fractures means that knowledge of fracture densities and other characteristics whenever available (along with the included fluid properties) could not be easily incorporated into realistic forward models of the conductivities, nor could inverse modeling be simply applied to interpretation of these same physical properties.

A current area of significant exploration and production effort, where such a theory is directly applicable is in the so-called "gas-shale" and "tight gas-sands." In both cases, a

significant portion of total porosity is due to cracks/fractures. One exploration problem for electromagnetic techniques (either borehole- or surface-based) is to be able to map areas with high gas saturation (resistive fractures relative to the background). A reasonable model of these cracks/fractures treats them (for example) as oblate spheroidal (*i.e.*, more or less penny-shaped — but at a macroscopically large size) holes filled with either conductive brine or resistive gas. Such highly conducting or resistive regions (even though quite small in volume compared to the overall volume of the reservoir) can create a locally anisotropic background for electromagnetic signals; and, if this set of fractures/cracks is oriented on average (as they very often are for reasons related to the anisotropy of the ambient tectonic and overburden stress fields), the electrical behavior of the overall system is therefore also likely to be anisotropic — both locally and possibly globally. Although useful analytical tools for modeling these situations have been available for some time, it seems that no work has yet been done to address these specific circumstances, and this gap in the literature provides one major motivation for the present work.

For electromagnetic surveys (both borehole and surface based) of earth media containing fluid-filled fractures, it is therefore necessary to understand and quantify the effects of either highly conductive or more resistive fluids residing in thin cracks or fractures fluid within the moderately conducting earth host. The main model we propose to consider will be that of thin fractures in the shape of oblate spheroids. These fractures can in principle be oriented any way in space, but because of the tectonic forces it is highly likely that on average the fractures of most interest will be oriented so that one of the two longer dimensions (of each approximately oblate-shaped spheroid) is vertical, while the only thin dimension is horizontal. It is not difficult, since the mathematics is virtually the same, to include the possibility in our studies of some of the fractures being oriented so both long dimensions are horizontal, while the thin dimension is vertical. It is somewhat harder to consider cases where the fractures are oriented arbitrarily in space, so this situation will not be a major emphasis of the following analysis, but such circumstances can also be treated straightforwardly with the methods under development here.

The ideas and tools used in this work are based in large part on some material outlined in Chapter 18 of Torquato (2002). This earlier work provides the needed physical and mathematical foundations, but the various specific cases studied here have not been treated previously by others, as far as the authors have been able to determine.

A general outline of the paper is: The following section on **Microstructure-based Constraints** provides a very brief review of the large literature on effective medium theories for the electrical conductivity problem in heterogeneous materials. The next section on **Effective Conductivity** introduces the equations for anisotropic conductive systems, mostly based on the textbook presentation in Torquato (2002). Some simple examples are discussed here to show explicitly how this method can be used to treat the problems of interest to us. The presentation is limited to cases of oblate spheroids (*i.e.*, ellipsoids having two large dimensions and one small dimension, like a pancake) here and throughout the paper — in part because this is the formulation emphasized by Torquato, and in part because (we postulate that) the behavior of most fracture systems of geophysical interest can be well-approximated by collections of thin oblate spheroidal inclusions. For the preliminary analyses of the present work, we place restrictions on cases considered in order to make some quick progress in the section **Simplifications for Diagonal Conductivities**. These choices reduce the number of possibilities to be studied drastically (otherwise we would need to consider all possible relative orientations of fractures and combinations thereof), and so it makes our self-assigned task possible to complete within a single journal article. Then the next section treats the well-known **Maxwell Approximation** [also see Milton (2002) and Torquato (2002)], which provides some convenient and very useful explicit formulas for comparisons to later results. The Maxwell approximation is sometimes called a "non-interaction formula," which (as will be discussed) is not an entirely accurate characterization.

Then, our main result which is the **Self-Consistent Generalization** for the anisotropic problem is presented. This approach requires updates of the effective overall background medium for high concentrations of inclusions. In order to check the usefulness of this particular nonlinear approximation scheme, its introduction is followed by a discussion of pertinent analytical methods of validating the computed results by making comparisons to various known rigorous bounding formulas such as the Weiner (1912) bounds and the Hashin-Shtrikman (1962) bounds.

Examples in the early parts of the paper are for conductive inclusions in a more resistive background medium. The section on **Results for Resisitive Inclusions** considers – within the same general analytical framework – what happens when the inclusions themselves are more resistive than the background (host) medium.

The significance and applicability of the crack density parameter ρ_c is emphasized in

the section on **Crack Density Analysis**. It is shown explicitly that — while this choice (or one of the other minor variants) of crack density measure is often useful for analyzing data — the concept of crack density should be understood as only an approximation to the actually very complex system behavior and therefore needs to be treated with some care when making general statements about such systems.

We conclude with a short discussion of some difficult problems having more general fracture orientation distributions, and also provide a **Worked Example for Three Distinct Fracture Sets**. Finally, some pertinent mathematical details are collected in the lone **Appendix**.

MICROSTRUCTURE-BASED CONSTRAINTS ON THE CHOICE OF AN EFFECTIVE MEDIUM THEORY

Before the work of Milton (1985), Norris (1985), Avellaneda (1987), and others in the mid-1980's, effective medium theories for the overall (or average) properties of composites were virtually always introduced for complicated heterogeneous-medium modeling problems without regard to the possibility of there being actual microstructures implicitly associated with each (or any) specific modeling choice. While not all effective medium theories do have implicit microstructures, it seems most appropriate to take advantage of this useful information whenever possible. In principle, it may be appropriate in some cases to design a near-optimal effective medium method when we know which microstructure it is that we want to mimic with our theoretical approach.

Prior to work in the early 1990's, the literature on elastic composites was in a state of confusion due to the observed fact that elastic behavior of aerogels and granular materials could **not** both be explained or modeled successfully by the same theory. The work of Berge *et al.* (1993) resolved this problem for the first time by showing that the cause of this confusion arose from misapplication of both the differential scheme and the self-consistent methods to problems incompatible with the true (and distinctly different) microstructures implicit in each of these two theories. This insight was attained by noting that the implicit microstructure of the solid constituent of an aerogel is compatable with that anticipated when using the differential effective medium approach (Norris, 1985; Avellaneda, 1987) for the elastic analysis. Similarly, the microstructure of a granular-like material such as fused-

glass beads is very similar to that being modeled by a self-consistent-style of analysis (Milton, 1985). Thus, a long-standing point of confusion in the effective medium theory literature was successfully resolved in the area of elastic-composites modeling simply by being careful to apply the theory with the most compatible implicit microstructure to each problem of interest.

An entirely analogous situation arises in the area of electrical conductivity modeling. There has been great success in modeling electrical (and also dielectric) behavior of granular media saturated with conducting fluids using (again) the differential effective medium scheme (Sen *et al.*, 1981; Norris *et al.*, 1985; Zimmerman, 1991; Berryman, 1995). The point to be emphasized here is that the pertinent microstructure of granular materials saturated with conducting fluids is completely analogous to that of the elastic aerogels in the elasticity application: in the elastic context, both the role and the actual shape of the solid component (which supports the elastic stresses and strains) is very similar geometrically (*e.g.*, completely analogous) to that of the conducting fluid in the pores of a granular material. So it seems very natural to imagine that the same type of theoretical approach (the differential scheme in particular) should work for both these applications, even though the physical contexts are quite different (elasticity versus electrical conduction). The implicit assumptions of the differential scheme are nevertheless virtually the same in these two cases. Our experience with modeling Archie's law in the geophysical context is that the differential scheme works very well, and does so at the small scales associated with Archie's law and borehole analysis because the theory and the physical problem both do have compatible microstructures.

However, the microstructure of an aerogel-like material is usually not appropriate for the applications of most interest to us in our present application. We are mainly trying to model macroscopic fractures containing either a more highly conducting fluid than the conductivity of the host (solid) medium, or (sometimes) possibly a more insulating fluid. So a differential scheme is expected to be less likely to give good results than a self-consistent scheme, based on perceived incompatibility (versus desired compatibility) of the respective implicit microstructures.

Because we are treating fractures having one thin dimension and two large dimensions throughout our following analysis, the main conducting paths in these systems will always be along the directions of these two longer dimensions (unless the pore-fluid itself is more insulating than the background). Also, if there happens to be a significant component of

surface conduction present in addition to the conductivity of the main saturating fluid, such components can be easily appended to the analysis by noting that the effective conductivity in the long dimensions is clearly in parallel (and therefore very easy to model for planar fractures) along with the main conduction paths being analyzed. In many cases, the surface conduction should provide a relatively small added contribution (whenever the surface layer itself can be assumed to be much thinner than the macroscopic fracture opening as should normally be true). The surface conduction enhancement to the effective conductivity in the two main directions of current flow for highly conducting pore-fluids is therefore expected to make only a very small contribution in this geometry. (One obvious exception to this scenario could be when the fluid in the fracture is very resistive, while there is also a very conductive surface layer which might then dominate the overall system conductivity. We shall not consider this special case further here.)

Related research along these lines continues to be developed (Berryman, 2009, 2010; Milton, 2012), and so it seems most appropriate to our goals to incorporate such ideas into the work presented here.

EFFECTIVE CONDUCTIVITY OF EARTH MEDIA CONTAINING MACROSCOPIC FLUID-FILLED FRACTURES

In the following presentation, we will typically be considering a single type of background conducting medium which will be labeled $j = 0$. There will also most often be three mutually orthogonal sets of macroscopic fractures, labeled $j = 1, 2, 3$, each of which contains the same type of conducting fluid. These sets of fractures may not however be present in equal concentrations, and therefore the results established in this way can easily become anisotropic. Deviations from our usual assumptions will be noted whenever appropriate. While there could be many different orientations of conducting fractures present in a real reservoir, it will become apparent that it is relatively straightforward to allow such general conditions. However, our present effort is focused on showing how the method works in some special cases while also demonstrating that the results obtained do satisfy a number of reasonable constraints, including for example satisfying certain rigorous bounding results for isotropic versions of the mostly anisotropic problems being considered.

Torquato (2000) (p. 462), Shafiro & Kachanov (2000), and/or Mavko *et al.* (2009) (pp.

414–417) show — using Torquato's notation — that the effective electrical conductivity of a medium containing conducting ellipsoids can be expressed as:

$$\sum_{j=0}^{3} \phi_j (\mathbf{\Sigma}_e - \sigma_j \mathbf{I}) \cdot \mathbf{R}^{(j,0)} = 0, \tag{1}$$

where $\mathbf{\Sigma}_e$ is the effective anisotropic (3×3 matrix or tensor) electrical conductivity of the target medium, having host (*i.e.*, background) scalar conductivity of σ_0, and inclusions all of which have conductivity σ_2, but nevertheless are composed of differently oriented fluid-filled fractures in our present application. The matrix $\mathbf{I}$ is the 3×3 identity matrix. Volume fractions ϕ_0 and ϕ_j are those of the host (0) and j-th inclusion ($j = 1, 2, 3$), where $\phi_0 + \sum_{j=1,2,3} \phi_j = 1$, by which we simply mean that the host and these fluid inclusions together fill the entire volume of space to be studied. The matrix

$$\mathbf{R}^{(j,0)} = \left[\mathbf{I} + \frac{\sigma_j - \sigma_0}{\sigma_0} \mathbf{A}_j \right]^{-1} \tag{2}$$

is called the "electric field concentration tensor" for an inclusion of type-j in the matrix material of conductivity σ_0, and the matrix $\mathbf{A}$ is the depolarization matrix for ellipsoidal inclusions defined in our Appendix, and in the references by Stratton (2007), and Torquato (2002). Recall that $\mathbf{R}^{(j,0)}$ is just equal to the identity matrix $\mathbf{I}$ if $\sigma_j = \sigma_0$, which is the host medium's value of conductivity. So $\mathbf{R}^{(0,0)} = \mathbf{I}$.

[Note: This first equation (1) in the paper is *not* our main result. It is a preliminary form to be modified later in order to produce the self-consistent version which is the main new result of this paper. Eq. (1) is actually one of several equivalent ways of writing the explicit Maxwell approximation, which will also be discussed in more detail in a later section. One important point however is to recognize now that here we are usually writing this Maxwell approximation for oblate spheroidal inclusions, while the most referenced version of the Maxwell approximation is normally written specifically for spherical inclusions.]

As explained in the **Introduction**, we limit consideration to some likely cases in which the fractures of interest are oriented either vertically, or horizontally. (Other cases can obviously be treated by rotating coordinates, but the possibilities quickly proliferate, and so we will not pursue this complication here.)

The diagonal depolarization tensor $\mathbf{A}_j$ has, for example when $j = 3$, the form:

$$\mathbf{A}_3 = \begin{bmatrix} Q_3 & & \\ & Q_3 & \\ & & 1 - 2Q_3 \end{bmatrix}, \tag{3}$$

where, for oblate spheroids (which is the only type of ellipsoid considered at the moment, but see a later section for discussion of the more general case), we have

$$Q_j = \frac{1}{2}\left\{1 + \frac{1}{(c/a)^2 - 1}\left[1 - \frac{\arctan(\chi_a)}{\chi_a}\right]\right\} \equiv Q, \tag{4}$$

with

$$\chi_a^2 = -\chi_c^2 = (a/c)^2 - 1, \tag{5}$$

and $\alpha \equiv c/a \leq 1$, so that c is the short-axis length, while a is the length of the other two axes for an oblate spheroid. When the spheroids all have the same aspect ratio, the value of $Q_j = Q$ is actually independent of j because it depends only on the shape of the ellipsoid — not on the fluid electrical conductivity σ_j within the ellipsoid, and also not on the orientation of the ellipsoid itself. Examples of Q for some specific values of aspect ratio α are: $Q = 0.036916$ for $\alpha = 0.05$, and $Q = 0.069604$ for $\alpha = 0.10$, and $Q = 0.098712$ for $\alpha = 0.15$.

If the oblate spheroid happens to be very flat, then $a/c \to \infty$ and therefore the value of $Q \to 0$. (We never actually take this limiting process all the way to zero, because then there would be no finite volume fraction to be associated with the fractures themselves, and the model would then not be internally consistent.) Thus, only one significant diagonal component in each of the $\mathbf{A}_j$'s would survive in this limit, and this component has the value of unity. It follows then, to a good approximation, that (2) for $j = 3$ implies the result in this limit $\sigma_2/\sigma_0 >> 1$, corresponding to:

$$\sigma_2 \mathbf{R}^{(3,0)} \simeq \begin{bmatrix} \sigma_2 & & \\ & \sigma_2 & \\ & & \sigma_0 \end{bmatrix}. \tag{6}$$

This provides some further insight into the meaning of the electric field concentration matrix (or tensor) and how it changes for the systems being studied here for different choices of the conductivity ratio σ_2/σ_0 (being inclusion conductivity over host conductivity).

While the scalar quantity $Q_j = Q$ itself is actually independent of the index j, the location of the distinct matrix elements along the matrix diagonal of $\mathbf{R}^{(j,0)}$ does depend on the index $j = 1, 2, 3$ — which is thereby indexing the type of oblate spheroid, *i.e.*, vertical-x, vertical-y, or horizontal-z. [Note: We use $x, y, z = 1, 2, 3$ to index the axis of symmetry of the oblate spheroids. The spheroids are termed "vertical" if one of the long dimensions is vertical; or "horizontal" if both of the long dimensions are horizontal.] So we consider two other distinct versions of (3), which are:

$$\mathbf{A}_1 = \begin{bmatrix} 1-2Q & & \\ & Q & \\ & & Q \end{bmatrix}, \tag{7}$$

and

$$\mathbf{A}_2 = \begin{bmatrix} Q & & \\ & 1-2Q & \\ & & Q \end{bmatrix}. \tag{8}$$

We see that the location of the diagonal element $1 - 2Q$ is determined by the value of j, while the other two diagonal matrix elements are given by Q itself.

Clearly other orientations are possible and will need to be considered in practice, but for a first pass through the theory and coding, we will consider only these simpler cases. For TTI (tilted transversely isotropic) systems, x, y, z can take on different meanings (not truly vertical and/or horizontal) within the tilted framework; while the math stays essentially the same as what is being presented here, but having to deal in addition with a rotated coordinate system.

The significance of these three matrices, $\mathbf{A}_1$, $\mathbf{A}_2$, $\mathbf{A}_3$, is easy to understand: The plane of the ellipsoid in (3) for $\mathbf{A}_3$, is the horizontal or xy-plane, having axis of symmetry direction z, which we take to be the vertical. In contrast, $\mathbf{A}_1$ has axis of symmetry x, while $\mathbf{A}_2$ has axis of symmetry y. We will be assuming (for present modeling purposes) that all of these ellipsoidal cracks are of the same basic oblate-spheroidal shape, but the volume fractions ϕ_j of each of these three types of fluid-filled fractures (or cracks) may differ. For example, we might have only vertical fractures. So, along with ϕ_0 which never vanishes, $\mathbf{A}_1$ and $\mathbf{A}_2$ for example might have non-zero values of ϕ_1 and ϕ_2. Or there might only be horizontal fractures in which case only ϕ_3 (and of course $\phi_0 \equiv 1 - \phi_1 - \phi_2 - \phi_3$) would be nonzero. In all cases, the total volume fraction must add up to unity, so $\sum_{j=0,1,2,3} \phi_j = 1$.

For the most general case being considered here, Eqn. (1) may be replaced by

$$\phi_0 \mathbf{\Sigma}_e \cdot \mathbf{R}^{(00)} = \phi_0 \sigma_0 \mathbf{I} + (\sigma_2 \mathbf{I} - \mathbf{\Sigma}_e) \cdot \sum_{j=1}^{3} \phi_j \mathbf{R}^{(j0)}. \tag{9}$$

Recall that $\mathbf{R}^{(00)} \equiv \mathbf{I}$. Also, note that we are assuming only one type of fluid constituent at a time, so all three types of fractures contain fluid having the same value of conductivity σ_2. [Note: This assumption greatly simplifies the current presentation – which will become complicated enough even so, but it is certainly *not* an absolute requirement of our general approach.]

Using the notation just introduced, we can now rewrite the expression for (1), dividing through by ϕ_0, which gives:

$$\mathbf{\Sigma}_e = \sigma_0 \mathbf{I} + \frac{1}{\phi_0} [\sigma_2 \mathbf{I} - \mathbf{\Sigma}_e] \cdot \sum_{j=1}^{3} \phi_j \mathbf{R}^{(j0)}. \tag{10}$$

Since $\mathbf{\Sigma}_e$ appears on both sides of this equation, we note that as written this is clearly an implicit equation for $\mathbf{\Sigma}_e$. One advantage of writing the equation this way arises from the realization that the fractures occupy a very small amount of space, and so their total volume fraction is quite small. Thus, for a very crude first approximation, we can assume that

$$\mathbf{\Sigma}_e \simeq \sigma_0 \mathbf{I}, \tag{11}$$

plus terms of order ϕ_j/ϕ_0 (relative volume fraction) times other terms depending on differences between host and inclusion conductivities. Clearly, this approximation is useless as a stopping point, but it is nevertheless a helpful starting point for an iteration scheme based on (10) — one that we expect will converge to the self-consistent result being sought here. Note that for the final iterative scheme we will obtain, the value of the background "constant" itself σ_0 does *not* remain constant, because the background as seen by the individual inclusions is changing on the average with each iteration, and in a cumulatively significance way.

[Note: Another distinct type of approximation called the differential effective medium (DEM) scheme could also be derived starting from an equation very similar to (10), but we will not pursue this option here. We make this choice based on the implicit microstructure known to be associated with this DEM approximation. [See Norris (1985) and Avellaneda

(1987)], who show the microstructure is sufficiently different from the microstructure envisioned here that we expect the results to be somewhat less useful than the ones we are considering. Also, see Sen *et al.* (1981) for isotropic examples.]

If we substitute (11) into the right hand side of (10), retrieve the result and then substitute this result again into the same right-hand-side, and so on, then we have a well-defined iterative process to find the effective $\mathbf{\Sigma}_e$ without having to solve directly the 3×3 matrix equation implied by (10). [Some readers may prefer to solve this matrix inversion problem in order to study explicitly the convergence characteristics of the iteration scheme. We prefer not to do this mostly because the use of such an iterative scheme itself tends to emphasize the reason for calling this method the **Self-Consistent Scheme**. Furthermore, the present formula is not a fully self-consistent scheme yet since it is very important to update the background conductivity $\sigma_0 \to \sigma^*$, as will be discussed at greater length later in the paper.] We expect (and also find in practice) that this iteration scheme converges quickly in almost all of the cases of interest, since by our assumptions σ_2 is significantly larger than the background σ_0, but also the fluid-filled–fracture volume fractions satisfy: $\phi_1 + \phi_2 + \phi_3 \ll \phi_0$. So, for reasonable ratios σ_2/σ_0 (*i.e.*, not differing too much from unity), each step in the iteration sequence should not produce a drastic change, and therefore the remaining steps are expected to produce a quickly converging result for the final value of $\mathbf{\Sigma}_e$. However, if the ratio σ_2/σ_0 is very large, additional care is required to obtain the desired accuracy.

The methods to be set out here include the Maxwell approximation and generalizations of the Maxwell approximation [see Torquato (2002)] for the conductivity of this anisotropic, fractured system. We can also produce other types of approximations, including self-consistent, differential effective medium, and various other generalizations. But, for an initial study of these systems, it seems wise to start with a simple choice of approximation (when available), which the present choice surely is. The next two sections therefore elaborate on the Maxwell approximation method, and then in the section on **Self-consistent Generalization of the Method for Higher Concentrations of Inclusions** we will show how to modify the method to make it into one example of a self-consistent effective medium theory for these same types of systems. These generalizations are not so important for low concentrations of inclusions, but can become vitally important when the inclusions are so dense that the field of each inclusion interacts in a significant way with the fields of close neighbors. So the results also depend then in a significant way on the crack/fracture

aspect ratio, as will be demonstrated.

Before embarking on our main studies here, one technical point of terminology should be clarified. We will sometimes use the terms Maxwell approximation and non-interaction approximation interchangeably in this paper. [Maxwell's approximation is defined carefully in the section entitled **Explicit Formulas for Σ_e: The Maxwell Approximation** which follows two sections after this one.] While this choice of language is correct for all the cases studied here involving fracture-shaped inclusions, it is not correct for some other shapes of inclusions. In particular, for spherical inclusion shapes, many authors — including for example Milton (2002) — have pointed out that Maxwell's approximation actually turns out to be identical to the results of Hashin-Shtrikman (1962) for coated spheres. Thus, for such inclusion shapes and composite geometries it is *not* correct to describe Maxwell's approximation as a noninteraction approximation. But with this caveat duly noted, we will nevertheless continue to use the terms Maxwell approximation and non-interaction approximation interchangably within the confines of the present paper since we never consider spherical inclusions directly in the present work.

SIMPLIFICATIONS FOR DIAGONAL CONDUCTIVITIES

Formula (10) is more general than is really needed to solve the special cases that we have discussed explicitly so far. If the fractures are not all perfectly aligned with the coordinate axes as they actually are assumed to be in the cases shown in Eqs. (3), (7), (8), then the formulas for the $\mathbf{A}_j$'s — and, therefore, for the $\mathbf{R}^{(j,0)}$'s — are no longer diagonal. But it is clearly advantageous to consider these special cases: (a) because they could in fact happen in practice, and (b) because they are so simple we can often write down formulas for the results, which helps our insight.

To provide examples of the $\mathbf{R}^{(j,0)}$'s, we have:

$$\mathbf{R}^{(3,0)} = \begin{bmatrix} \frac{1}{1+[(\sigma_2-\sigma_0)Q_3/\sigma_0]} & & \\ & \frac{1}{1+[(\sigma_2-\sigma_0)Q_3/\sigma_0]} & \\ & & \frac{1}{1+[(\sigma_2-\sigma_0)(1-2Q_3)/\sigma_0]} \end{bmatrix} \tag{12}$$

and

$$\mathbf{R}^{(1,0)} = \begin{bmatrix} \frac{1}{1+[(\sigma_2-\sigma_0)(1-2Q_1)/\sigma_0]} & & \\ & \frac{1}{1+[(\sigma_2-\sigma_0)Q_1/\sigma_0]} & \\ & & \frac{1}{1+[(\sigma_2-\sigma_0)Q_1/\sigma_0]} \end{bmatrix}. \tag{13}$$

The third case [*i.e.*, $\mathbf{R}^{(2,0)}$] is easy to deduce from the forms of the two shown here. Rather than showing the full result again, we will show instead a very useful approximate form when $\sigma_2 >> \sigma_0$ (*i.e.*, very conductive inclusion in a moderately conductive host), which is:

$$\mathbf{R}^{(2,0)} \simeq \left(\frac{\sigma_0}{\sigma_2}\right) \begin{bmatrix} \frac{1}{Q_2} & & \\ & \frac{1}{1-2Q_2} & \\ & & \frac{1}{Q_2} \end{bmatrix}. \tag{14}$$

Our main point is that, since in all these cases the $\mathbf{R}^{(j,0)}$'s are diagonal, the effective conductivity $\mathbf{\Sigma}_e$ we seek to determine must also be diagonal. We find easily that the final result can then be written in several (all useful) equivalent forms, one of which is:

$$\mathbf{\Sigma}_e = \sigma_0\mathbf{I} + (\sigma_2 - \sigma_0)\frac{1}{\phi_0}\sum_j \phi_j \mathbf{R}^{(j0)} \times \left[\mathbf{I} + \frac{1}{\phi_0}\sum_j \phi_j \mathbf{R}^{(j0)}\right]^{-1}. \tag{15}$$

Another alternative we make use of is:

$$\mathbf{\Sigma}_e = \sigma_2\mathbf{I} + (\sigma_0 - \sigma_2) \times \left[\mathbf{I} + \frac{1}{\phi_0}\sum_j \phi_j \mathbf{R}^{(j0)}\right]^{-1}. \tag{16}$$

It has generally been found to be a good idea to start with the largest conductivity value and perturb around that value, as convergence of our scheme is usually more rapid under these circumstances. So Equation (16) is perhaps the most attractive of these formulas for very conductive inclusions in a more resistive background medium, because it emphasizes the influence of σ_2, which is the conductivity of the fluid in the fractures. When the fluid conductivity is high, the result (16) is then expected to be substantially more highly conducting than the surrounding earth materials. This formula is also somewhat shorter to write, and therefore easier to code. Alternatively, if the host is the most conductive component and the inclusion conductivity is much smaller, then (15) may often be the preferred alternative. Finally, note that both of these forms are entirely equivalent to (10).

There is some remaining algebra needed to find a simple programmable formula for the effective conductivity. However, this is all very straightforward, so the details will *not* be shown here.

The final result is most conveniently written in terms of two constant scalar factors: A and B. These factors are:

$$A^{-1} = \frac{1}{\sigma_2 - \sigma_0} + \frac{1 - 2Q}{\sigma_0}, \tag{17}$$

and

$$B^{-1} = \frac{1}{\sigma_2 - \sigma_0} + \frac{Q}{\sigma_0}, \tag{18}$$

where Q was defined previously in (4). Then, we find that

$$-(\sigma_2 - \sigma_0) \times \sum_{j=1,2,3} \phi_j \mathbf{R}^{j0} = \begin{bmatrix} \phi_1 A + (\phi_2 + \phi_3)B & & \\ & \phi_2 A + (\phi_3 + \phi_1)B & \\ & & \phi_3 A + (\phi_1 + \phi_2)B \end{bmatrix}, \tag{19}$$

and, therefore, the **Maxwell approximation** for $\mathbf{\Sigma}_e$ is given explicitly by

$$\mathbf{\Sigma}_e = \sigma_2 \mathbf{I} - \phi_0 (\sigma_0 - \sigma_2)^2 \times \begin{bmatrix} D & & \\ & E & \\ & & F \end{bmatrix}, \tag{20}$$

where

$$\begin{aligned} D^{-1} &= \phi_0(\sigma_2 - \sigma_0) + \phi_1 A + (\phi_2 + \phi_3)B, \\ E^{-1} &= \phi_0(\sigma_2 - \sigma_0) + \phi_2 A + (\phi_3 + \phi_1)B, \\ F^{-1} &= \phi_0(\sigma_2 - \sigma_0) + \phi_3 A + (\phi_1 + \phi_2)B. \end{aligned} \tag{21}$$

With these definitions, we see that the formula (20) reduces correctly to $\Sigma_e = \sigma_2 \mathbf{I}$ if $\phi_1 = \phi_2 = \phi_3 = 0$, as it should. If $\sigma_2 \to \sigma_0$, both A and B approach $(\sigma_2 - \sigma_0)$, so D, E, and F all approach $1/(\sigma_2 - \sigma_0)$, and therefore $\mathbf{\Sigma}_e \to [\phi_0 \sigma_0 + (1 - \phi_0)\sigma_2]\mathbf{I}$. This limit is exactly the Wiener (1912) upper bound on conductivity for these systems [see the section on **Approaches to Validation of Effective Medium Formulas** (two sections on) for more discussion], and it is also what would be expected for conductors in series, or resistors in parallel. So this result clearly has the right ultimate limit as $\phi_0 \to 1$.

To gain some further insight into the meanings of these formulas and the significance of the Maxwell approximation, consider an example for brine-filled fractures in a typical sand environment with $\sigma_2/\sigma_0 \simeq 0.003$ to 0.3. Then, $A \simeq \sigma_0/(1-2Q)$ and $B \simeq \sigma_0/Q$. If $Q \simeq 0.01$ or less (as might be consistent with a flat crack geometry), then the only terms in (21) that survive having any significant magnitude are the leading terms, all of which give the same result $\simeq \phi_0(\sigma_2 - \sigma_0)$, together with the terms proportional to $B \simeq 100\sigma_0$ — which may often (but not always) be negligible, since σ_0/σ_2 typically may be small ($\simeq 0.003$ to 0.3). Then, we find that

$$D \simeq \frac{1}{\phi_0(\sigma_2 - \sigma_0)} \left[1 - \frac{\sigma_0}{\phi_0(\sigma_2 - \sigma_0)} \left(\frac{[\phi_2 + \phi_3]}{Q} + \frac{\phi_1}{1 - 2Q} \right) \right], \tag{22}$$

together with analogous (*i.e.*, permuted) expressions for E and F. The last term on the right side of this expression is generally negligible because $(1 - 2Q) >> Q$. These facts lead to the conclusion that (20) is nearly isotropic, and has a value not very different from the isotropic σ_0 value, so that

$$\mathbf{\Sigma}_e \simeq \sigma_0 \mathbf{I} + \left(\frac{\sigma_0}{\phi_0 Q} \right) \begin{bmatrix} (\phi_2 + \phi_3) & & \\ & (\phi_3 + \phi_1) & \\ & & (\phi_1 + \phi_2) \end{bmatrix}. \tag{23}$$

We mean by this statement to emphasize only that it is much closer to the background value σ_0 than to inclusion value σ_2 in all three directions. [Note that the factor of Q in (23) guarantees a substantial correction, which can in some cases be on the same order as $\sigma_2/\sigma_0 \simeq 0.03$.] This result is only somewhat larger than the host value σ_0 due to the presence of the highly conducting inclusions, but curiously *the formula is still independent of the actual value of* σ_2. There is nevertheless an enhancement in the conductivity due to the small value of Q in the denominator of the second term. These results are definitely *not* the end of our story, but they tell us that a good starting approximation to the final result will nevertheless be $\mathbf{\Sigma}_e = \sigma_0 \mathbf{I}$, plus these smaller anisotropic corrections.

If $\sigma_2 >> \sigma_0$ (as is being assumed either for conductive brine inclusions in a basalt or for a dry sand host) and the volume fraction of fractures remains small, then the effect of the inclusions is felt more strongly through the decrease in the volume fraction associated with σ_0 than with the actual value of the fluid conductivity σ_2 itself. This fact will prove to be very useful to us in the following sections concerning *self-consistent extensions* of these results.

Another important feature of (23) that should be emphasized is that diagonal components of the matrix displayed here can all be written in the general form: $(\overline{\phi}_2 - \phi_j)$, where j is the index of particular diagonal matrix element (and where the total porosity is $\overline{\phi}_2 \equiv \phi_1 + \phi_2 + \phi_3$). This behavior is the result of the contributions to conductivity in the j-th direction coming specifically from the other two fracture sets, *i.e.*, the ones whose axes of symmetry are orthogonal to the j-th direction. These same types of permuted contributions to the electrical behavior will be observed for the more sophisticated theories developed in the following sections. This type of behavior is of significance in all our final results, because we find that these systems have a tendency to average themselves out — thus becoming more isotropic in their overall behavior than might be expected from the range of values found in the respective porosities ϕ_1, ϕ_2, and ϕ_3. In particular, the diagonal matrix elements in (23) can all be written in the form $(\overline{\phi}_2 - \phi_j)$ for $j = 1, 2, 3$, respectively, showing that the leading contribution in each element is the total porosity – thus, providing an explicit example and a partial clarification of this observed averaging behavior.

Finally, we should emphasize that the absence of contributions from σ_2 in (23) is strictly a low-volume fraction, noninteraction approximation result. In contrast, we will find strong contributions from the fluid electrical conductivity in our later results.

SELF-CONSISTENT GENERALIZATION OF THE METHOD FOR HIGHER CONCENTRATIONS OF INCLUSIONS

We will now introduce a different generalization of the proposed method that will permit its use in cases of higher concentrations of good conductors in a more insulating background medium. The value of this alternative approach is greatest when the sum of all the volume fractions of the more highly conducting inclusions is large. One general rule of thumb is that a self-consistent method should surely be considered if $\phi_1 + \phi_2 + \phi_3 \geq 0.5$, because then the interactions among all the inclusions must be important. But we can also test the importance at smaller volume fractions by first formulating the self-consistent theory, trying it at increasingly higher inclusion concentrations, and then noting when the results start to deviate significantly from the results for noninteracting inclusions. This procedure will be the one followed in our examples.

Before traveling this path, we should perhaps provide an explanation of why we are choos-

ing one approach instead of some other well-known method such as the differential effective medium (DEM) scheme (Sen *et al.*, 1981; Norris, 1985; Norris *et al.*, 1985) that has been used extensively for generally isotropic electrical/dielectric problems previously. The two main methods usually considered are the self-consistent (SC) or — more specifically — the CPA (coherent potential approximation), versus the DEM approach. Both of these classes of methods are known to be realizable, by which we mean that the method of generating the numerical values is consistent with an actual possible microstructure (though not necessarily the microstructure we want!). Milton (1985) demonstrated realizability for CPA and Avellaneda (1987) demonstrated realizability for DEM. This realizability condition, once proven, gives users confidence that the method does not ever give absurd results.

The values coming out of such a realizable theory will always be physical, by which we mean they lie within or on the known rigorous bounds. The point for us now is that these two methods, although both are realizable, do not correspond to the same microstructures. (Since they clearly do not give the same results, this fact provides one sensible way of distinguishing the method of choice.) We need to choose carefully which of these two (or among others if others were available) to use for our particular application. For example, it is known in the elastic modeling context (Berge *et al.*, 1993; Berryman and Berge, 1996; Berryman *et al.*, 2002) that the CPA or SC method tends to correspond to a material like a sandstone or sintered glass-bead structure (in which pores may be connected or unconnected depending on grain shapes and overall porosity content), while — in contrast — the DEM tends to correspond to an aerogel type of structure, having thin filaments of solid and connected pore-space at all volume fractions.

So, the approach we now choose is a common one (Stroud, 1975; Torquato, 2002) for generalizing noninteracting approximations to self-consistent approximations. The concept is this: we assume that each bit of conducting material in the medium of interest is actually imbedded in the effective (now self-consistent) overall anisotropic (matrix) conductivity $\mathbf{\Sigma}^*$. We use the $*$ superscript to designate the self-consistent (or SC) approximation. Then equation (1) becomes

$$\sum_{j=0}^{3} \phi_j (\mathbf{\Sigma}^* - \sigma_j \mathbf{I}) \cdot \mathbf{R}^{(j*)} = 0, \tag{24}$$

and equation (2) becomes

$$\mathbf{R}^{(j,*)} = \left[\mathbf{I} + \frac{\sigma_j - \sigma^*}{\sigma^*} \mathbf{A}_j \right]^{-1}, \tag{25}$$

which is now called the electric field concentration tensor for an inclusion of type j in the matrix of (average) isotropic conductivity σ^*.

Note that we are now making one further approximation in (25) by introducing an average isotropic σ^*, which is defined by

$$\sigma^* \equiv \frac{1}{3}\mathbf{Tr}\boldsymbol{\Sigma}^* = \frac{\sigma_1^* + \sigma_2^* + \sigma_3^*}{3}, \tag{26}$$

where

$$\boldsymbol{\Sigma}^* = \begin{bmatrix} \sigma_1^* & & \\ & \sigma_2^* & \\ & & \sigma_3^* \end{bmatrix}. \tag{27}$$

It is not immediately obvious that this approximation is legitimate; however, the final calculations in the previous section on **Explicit Formulas for Σ_e: The Maxwell Approximation** that lead to (23) have shown explicitly that these results, for relatively low volume fractions of such fractures in an isotropic host medium, will in fact be close to isotropic to a very good first approximation. In particular, we see that (23) implies:

$$\sigma^* \simeq \sigma_0 \left[1 + \frac{2}{3\phi_0 Q}\left(\phi_1 + \phi_2 + \phi_3\right)\right] = \sigma_0 \left[1 + \frac{2}{3\phi_0 Q}\left(1 - \phi_0\right)\right]. \tag{28}$$

When we need to distinguish this approach from a fully self-consistent method (*i.e.*, one that starts by assuming the background medium is itself anisotropic and then carries out the fully anisotropic self-consistent calculation), we will call the present approach the "weakly self-consistent approximation" and its more rigorous alternative the "fully self-consistent approximation." We treat only the weakly self-consistent approximation in this section, but generalize to the fully self-consistent approximation in the section on **Worked Example for Three Distinct Fracture Sets**.

For further clarification, when $j = 0$, the diagonal depolarization tensor $\mathbf{A}_0$ associated with the background (host) material has the form:

$$\mathbf{A}_0 = \frac{1}{3}\mathbf{I}, \tag{29}$$

because we have chosen to treat the *host medium* as if it were composed entirely of conducting spheres of all sizes as is required in order to fill up the space not occupied instead by the fractures filled with either higher or lower conductivity fluid. This approach is justified in part both because it is very convenient, and also because it is completely in line with the

model we are using. This fact follows because the host medium is assumed to be isotropic, and also because a truly isotropic medium can be decomposed into isotropic chunks of any shape (or size) we might choose. The spherical shape is surely the most convenient choice to make, and it is also one of the most commonly studied cases in all effective medium theories. So this case can be considered to be very well-understood.

The method just described has been implemented, and gives reasonable estimates of the anisotropic conductivity, but it can also take many iterations to converge. Even so this is not much of a drawback, since this process still takes very little computational (or real user) time. We will present some alternative methods later in the paper that can also be used to help to validate the self-consistent method as presented here for the anisotropic case.

Although it would be natural to present some examples of the methods just discussed at this point in the paper, it will prove beneficial to delay such results until the section on **Crack Density Analysis**, where we can make more comparisons. For now, we need to develop some other ideas first, so we can take full advantage of the concept of crack density (soon to be introduced here) in the presentation of some of the following illustrations.

APPROACHES TO VALIDATION OF EFFECTIVE MEDIUM FORMULAS

So far we have presented methods for computing effective medium estimates of electrical conductivity for systems having sets of oriented conducting-fluid–filled fractures, all having the same shape (oblate spheroids) and the same aspect ratio. This situation is not expected to be totally realistic in the earth, but it is important for us to study this case first so we can find useful and meaningful ways to validate this class of methods and results. One known means of accomplishing this validation goal would be to resort to full-scale numerical modeling. However, we are attempting to avoid that approach here by developing some less computationally intensive methods, especially by making use of known rigorous bounds. But this method is also somewhat problematic since the majority of the known bounds (except for layered materials) are generally written down only for overall isotropic composites. So one way to check our results within the same sets of computations that we are already defining and implementing here is to consider cases that do reduce to isotropic results so they can then be checked relatively easily. The results in some cases are therefore cast in a way to make comparisons to such rigorous bounds on conductivity for random — but

isotropic — composites.

There are presently two distinct types of known conductivity bounds (Torquato, 2002, p. 557): Wiener (1912) bounds and Hashin-Shtrikman (1962) bounds on the conductivity. [Also see Brown (1955) for a pertinent review and discussion of the limitations of the earlier methods.] The Wiener bounds are simply the arithmetic (upper, +) and harmonic (lower, −) means, respectively, of the constituent conductivities based on volume fractions:

$$\sigma_W^+ = \phi_0\sigma_0 + \overline{\phi}_2\sigma_2, \tag{30}$$

and

$$\sigma_W^- = \left(\frac{\phi_0}{\sigma_0} + \frac{\overline{\phi}_2}{\sigma_2}\right)^{-1}, \tag{31}$$

where $\phi_0 + \overline{\phi}_2 = 1$. So these are very easy to implement.

The Hashin-Shtrikman bounds on conductivity for three-dimensional isotropic composites with only two constituents are:

$$\sigma_{HS}^+ = \sigma_W^+ - \frac{\phi_0\overline{\phi}_2(\sigma_0 - \sigma_2)^2}{\langle\tilde{\sigma}\rangle + 2\sigma_2}, \tag{32}$$

and

$$\sigma_{HS}^- = \sigma_W^+ - \frac{\phi_0\overline{\phi}_2(\sigma_0 - \sigma_2)^2}{\langle\tilde{\sigma}\rangle + 2\sigma_0}, \tag{33}$$

where

$$\langle\tilde{\sigma}\rangle \equiv \phi_0\sigma_2 + \overline{\phi}_2\sigma_0. \tag{34}$$

Neither of these pairs of bounds (Weiner and Hashin-Shtrikman) distinguishes between host and inclusion phases, both phases being treated equally. But in our present modeling, we consistently treat σ_0 as the host (*i.e.*, the earth medium within which inclusions are imbedded), and σ_2 as the inclusion phase (*i.e.*, conducting fluid in the fractures). So for highly conductive inclusions we typically have $\sigma_0 << \sigma_2$, while $\sigma_2 << \sigma_0$ for the highly resistive inclusions, and $\overline{\phi}_2 < \phi_0$ (inclusions occupy a significantly smaller volume than the host) in all our modeling examples. These restrictions on the conductivity values are the reasons for the explicit σ_2 contribution in the denominator of (32) and also for the explicit σ_0 contribution in the denominator of (33). If instead $\sigma_2 < \sigma_0$, then the stated roles of (32) and (33) are reversed.

For the oriented inclusions in our earlier modeling examples, we treated all the inclusions as having the same aspect ratio, but possibly having different volume fractions. To bring this

modeling into line with these rigorous bounds, what we need to do now is set the three volume fractions of the inclusions equal to each other so that $\phi_1 = \phi_2 = \phi_3$ and $\overline{\phi}_2 \equiv \phi_1 + \phi_2 + \phi_3$. And, of course, then we also have $\phi_0 = 1 - \overline{\phi}_2$. Having equal concentrations of the each of the three types of oriented (x,y,z-axes of symmetry, respectively) guarantees that the model will produce an overall isotropic conductivity model. So these computed results can then be compared directly with the (presumably) rigorous bounds.

Examples follow in Figures 1, 2, and 3. The units of the ordinate in all the Figures has been normalized so as to cover the range of values expected from that of highly ionized sea water $\sigma \simeq 5$ S·m^{-1} to that of deionized water having $\sigma \simeq 5 \times 10^{-6}$ S·m^{-1}.

In related work we have found that, for very small aspect ratios such as $\alpha = 10^{-5}$, the SC estimates are important all the time. Except for this warning and the following very brief discussion, we will not be reporting on this additional work in detail here. When the fractures have such small aspect ratios, we deduce that the reason for this result is that the fracture number density then becomes very high and the fracture relative spacing correspondingly becomes very low for a fixed value of porosity, but decreasingly small aspect ratio. So self-consistency becomes very important in order to account approximately for the many close interactions among the numerous small-aspect-ratio fractures.

The cases considered in greater detail here range from $\alpha = 0.05$ to 0.15. For $\alpha_1 = 0.05$, SC is important for $\overline{\phi}_2 \simeq 0.01$ and higher. For $\alpha_2 = 0.10$, SC is important for $\overline{\phi}_2 \simeq 0.03$ and higher. For $\alpha_3 = 0.15$, SC is important for $\overline{\phi}_2 \simeq 0.06$ and higher.

The most important general observation to be made about Figs. 1–4 is this: *neither the Wiener nor the Hashin-Shtrikman bounds depend on the actual shapes of the inclusions*, while clearly *both* the Maxwell (noninteraction) estimates and the self-consistent estimates *do depend significantly on these inclusion shapes*. Thus, as formulated, the results depend on two distinct types of parameters: porosity and aspect ratio. One natural question that we can consider then (and the section on **Crack Density Analysis** will treat this issue in detail) is whether or not it might be possible to reduce the number of independent parameters. This issue leads to a discussion of the crack density parameter (*i.e.*, porosity divided by aspect ratio), which is also elaborated further in the section on **Crack Density Analysis**. Note that the crack density concept was introduced into the geophysics literature by O'Connell and Budiansky (1977), and earlier in the context of conductivity modeling by Bristow (1960).

RESULTS FOR RESISTIVE INCLUSIONS

Results for contrasting cases having inclusions that are more resistive (less conductive) than the host medium are presented in Fig. 5. The results shown are only for the Maxwell approximation. Results for the self-consistent approach have also been tested for these same cases, but the SC results appear to be generally unsatisfactory. The most obvious problem is that, for cases having crack density $\rho_c = \phi/\alpha \geq 0.2$, we have found that the iteration scheme for the SC method actually does not ever converge. For values of $\rho_c < 0.2$, the SC approximation does converge, but the result obtained is always the same for all porosities and it is more conductive than that of the of host medium. This result is not therefore reasonable on physical grounds, because introducing less conductive material into the composite cannot make the composite more conductive. These results do not necessarily imply that there is no self-consistent scheme that will work for these problems – only that we have not found a workable scheme so far. Therefore, we do not recommend use of the present self-consistent method for resistive inclusions in a more conductive background medium.

A likely reason for the convergence problems observed in this case has to do with the use of the approximation (26) in (25). When the inclusions are highly conducting, this approximation leads to satisfactory results, since then some thin highly conducting fractures do not significantly affect the overall system conductivity in the directions perpendicular to these conducting planes. However, when the inclusions are highly insulating, this approximation does significantly perturb the overall system behavior, since it makes little difference how thin (as long as this thickness remains finite) the fractures are if their saturating fluid is either a non- or a very poor-conductor. The result is then dominated by this approximation, and so it is not recommended for such cases having insulating fluids in the fractures.

Until a more universally acceptable SC scheme can be formulated for these cases, we recommend instead using the Maxwell approximation for this subset (resistive inclusions in a more conducting host) of problems. The results obtained with this Maxwell method seem perfectly reasonable on physical grounds, and should be useful estimates as long as the volume fractions do not become unreasonably large. The Maxwell approximation is a perturbation result, and therefore requires "small" (in some sense that is not always immediately obvious how to quantify) volumes of inclusions for it to be valid. So where very large volume fractions of inclusions are present, this method should not be used, and we do

not have a suitable alternative (short of full-blown computer modeling) to suggest at the present time.

CRACK DENSITY ANALYSIS

The curves plotted in Figs. 1–3 have been displayed as a function of the volume fraction of the highly conducting fluid inclusions. The results show that there is no universal behavior in evidence when the results are studied and presented this way. Next we have two important parameters to consider: (1) the volume fraction and (2) the aspect ratio of the cracks. It has been found useful in studies of other physical systems to recognize that there is another way to display these curves in a more robust and universal form, namely by treating the curves as functions of a single parameter. One good choice for this single parameter has been shown by Bristow (1960), O'Connell & Budiansky (1973), Hudson (1981), Shafiro & Kachanov (2000), Grechka (2005), Grechka and Kachanov (2006a,b), and others including (Berryman & Grechka, 2006; Berryman, 2007; Berryman, 2008; Aydin & Berryman, 2010) to be the crack density, defined (for example) by the ratio $\rho_c \equiv \phi/\alpha$. [This particular choice of definition for ρ_c is not universal, as some authors prefer to include additional numerical factors. Hudson (1981), for example, defines a crack density parameter for applications to elasticity by $\rho_e \equiv 3\rho_c/4\pi$, which differs from our present choice of definition for conductivity applications only by a constant factor of $3/4\pi$. Any of these (and some other) common choices for the definition of crack density is equally valid as long as each is used consistently, and not confused with one of the other viable choices.]

The fundamental idea behind all these choices of crack density parameter is that each crack contributes to the overall electrical behavior in a way that depends more importantly on the number of cracks than it does on the total volume occupied by the cracks. [A simple analog description might be to say that these fluid-saturated cracks act somewhat like thin electrically conducting wires in a resistor network, where the detailed geometry of individual "wires" themselves is not as important as such simple measures as the length and the cross-sectional area of these "wires."] In fact the crack density concept was first introduced for electrical conduction problems by Bristow (1960) and only later for applications to elasticity by O'Connell & Budiansky (1973). See Berryman (2008) for some further discussion of these relationships.

To test the idea, we now replot the results in Figures 1 and 2 in the way suggested. Figure 3 shows the replotted results for the Maxwell (noninteraction) approximation. Here we see that the results do in fact seem to fall along a more universal curve than they did before. Figure 4 shows the replotted results for the self-consistent approximation. Here we see that the results for smaller porosities and also smaller crack densities still line up well, as they did in Figure 3.

[Another case treated (but not discussed in detail here) having very small aspect ratio ($\alpha_1 = 10^{-5}$), shows that the resulting curve does not line up at all well with these other curves. One possible explanation for this misalignment is related to the fact that the strong interactions observed in this case led to the conductivity estimates being slightly higher than the Hashin-Shtrikman upper bounds, though still remaining below the Wiener bounds. This behavior seemed to indicate that this limit is very tightly constrained in its range of reliable values, and therefore we concluded this case was too extreme to be discussed further here. We had considered this case initially to provide one test of the limits of the various theories considered, and indeed we seem to have succeeded in finding some of those limitations.]

It may also be worthwhile to note that the arguments usually made concerning the importance of the crack density have typically been used for cases where the cracks themselves were actually voids. Thus, for the case of elastic analysis, these empty cracks are holes, maximally weakening the overall response to elastic compression and extension. Similarly, for electrical analysis, empty cracks are essentially perfect insulators, and electrical current must flow around these obstacles. What has been shown here for the most part is the reverse situation, where the cracks are more highly conducting than the surrounding material, and is showing that the analogous process is also true in which the current tends to be focused more tightly through the conducting fluid-filled cracks; and the concept of the crack density $\rho_c = \phi/\alpha$ again captures the main behavior of the system in many (but not all) circumstances. Also see Rocha & Acrivos (1973a,b) and Chen (1976) for further discussion.

The curves in the three Figures 6–8 present the results of nine distinct numerical experiments. The point of these displays is to show how each of the diagonal components of the conductivity matrix can vary with crack density defined as $\rho_c = \phi/\alpha$. To provide some control (so we are comparing objects being somewhat alike), the three cases considered all have the same total porosity: $\overline{\phi}_2 = \phi_1 + \phi_2 + \phi_3 = 0.333$. For the first case (Fig. 6), we have: $(\phi_1, \phi_2, \phi_3) = (0.022, 0.111, 0.200)$. For the second case

(Fig. 7), we have: $(\phi_1, \phi_2, \phi_3) = (0.089, 0.111, 0.133)$. For the third case (Fig. 8), we have: $(\phi_1, \phi_2, \phi_3) = (0.067, 0.111, 0.155)$. The resulting models are clearly anisotropic since $\sigma_1^* \neq \sigma_2^* \neq \sigma_3^*$, etc., in all three cases. Figure 6 shows the diagonal component σ_2^*; Figure 7 plots the diagonal component σ_1^*; and Figure 8 plots the diagonal component σ_3^*. We end up with nine different numerical experiments because, in addition to variable volume fractions ϕ_j, we also have variable aspect ratios: α_1, α_2, and α_3.

The main message here is that, in Figures 7 and 8, we see almost linear variation of the conductivities σ_j^* when plotted versus crack density ρ_c, which is directly proportional to porosity ϕ for fixed aspect ratio. Behavior in Figure 6 however appears to be quite different, but porosity $\phi_2 = 0.111$ is constant, and so the only variable is aspect ratio α. The behavior in Figure 6 is therefore actually completely consistent with that of the other two Figures in this set, since each cluster of three points has exactly the same porosity, aspect ratio, and crack density. This shows again (and the result is especially clear in Figure 6) that crack density is a good (but not perfect!) measure of the most important dependencies contained in ϕ and α. Total observed spread in these plotted values is about 2 out of 200, so this indicates a 1% error is typical for these particular examples. Errors of this small magnitude are usually well tolerated in typical applications to earth systems.

If we wanted to claim that different models having the same crack density also have about the same conductivity, the Figure 6 shows in this fashion that the quantitative error of such a qualitative assertion is about 1% (at least in these examples).

The crack density approach is certainly not the only possible way analyze data of this type. Another useful approach (which we will not discuss here) as developed by Herrick and Kennedy (1994) introduces a measure of electrical efficiency that is also related to pore geometry and tortuosity of the highly conducting phase.

FURTHER GENERALIZATIONS: ANISOTROPIC MAXWELL APPROXMATIONS

Some of the models that have been presented might seem rather inflexible. In particular, we have considered so far only cases with sets of fractures wherein all the fractures are oblate spheroids having the same aspect ratio. A more versatile model is surely of interest for general field applications, and this section will discuss various types of generalizations

that are possible within the framework already discussed. Two types of generalizations will be treated: We consider alternatives such that (1) all three types of fractures (two vertical and one horizontal) are still oblate spheroids, but possibly having different aspect ratios; and/or (2) two of the three fracture sets lie at oblique angles to each other (being neither exactly parallel nor exactly perpendicular).

Three (or more) different aspect ratios

Having different aspect ratios in the various fracture sets is clearly both possible, and even very likely to happen in practice. In fact, this generalization of the presented model is both very easy to introduce and also easy to execute in computer code. (For this first exercise, we still assume that all three fractures sets are mutually orthogonal but consider violations of this constraint in the next subsection.)

Recalling the forms of Eqs. (3), (4), and (5), we see that a generalization permitting differing aspect ratios is entirely straightforward. We still assume that the fractures themselves are oblate spheroids, but there is no difficulty involved in assuming that there are three (or quite possibly many more — and therefore a distribution of aspect ratios would need to be considered) distinct aspect ratios present, so that (4) and (5) are replaced by:

$$Q_j = \frac{1}{2}\left\{1 + \frac{1}{(c_j/a_j)^2 - 1}\left[1 - \frac{\arctan(\chi_{aj})}{\chi_{aj}}\right]\right\} \quad \text{for} \quad j = 1, 2, 3, \ldots, \tag{35}$$

where

$$\chi_{aj}^2 = (a_j/c_j)^2 - 1. \tag{36}$$

Limiting the present discussion to only three distinct types, and then making use of these values, we have:

$$\mathbf{A}_1 = \begin{bmatrix} 1 - 2Q_1 & & \\ & Q_1 & \\ & & Q_1 \end{bmatrix}, \tag{37}$$

$$\mathbf{A}_2 = \begin{bmatrix} Q_2 & & \\ & 1 - 2Q_2 & \\ & & Q_2 \end{bmatrix}, \tag{38}$$

and

$$\mathbf{A}_3 = \begin{bmatrix} Q_3 & & \\ & Q_3 & \\ & & 1-2Q_3 \end{bmatrix}. \tag{39}$$

We are still assuming that the fractures are conveniently aligned with respect to the xyz-axes. If this is not the case, then — for whichever set or sets of fractures are misaligned — we need to rotate the corresponding $\mathbf{A}_j$ (by which we mean that $\mathbf{A}_j$ becomes a full matrix having six distinct nonzero components, rather than a diagonal matrix having only three nonzero components), so it has the proper orientation relative to the external coordinate axes. We shall not pursue these complications here, but they are straightforward to handle in code.

To obtain the pertinent explicit (Maxwell) formulas for the conductivity, we need to generalize (17) and (18) so that, for $j = 1, 2, 3$:

$$A_j^{-1} = \frac{1}{\sigma_2 - \sigma_0} + \frac{1-2Q_j}{\sigma_0}, \tag{40}$$

and

$$B_j^{-1} = \frac{1}{\sigma_2 - \sigma_0} + \frac{Q_j}{\sigma_0}, \tag{41}$$

where Q_j was defined previously by (35) and (36). Then, we find that

$$-(\sigma_2 - \sigma_0) \sum_{j=1,2,3} \phi_j \mathbf{R}^{j0} = \begin{bmatrix} \phi_1 A_1 + \phi_2 B_2 + \phi_3 B_3 & & \\ & \phi_2 A_2 + \phi_3 B_3 + \phi_1 B_1 & \\ & & \phi_3 A_3 + \phi_1 B_1 + \phi_2 B_2 \end{bmatrix} \tag{42}$$

and, therefore,

$$\mathbf{\Sigma}_e = \sigma_2 \mathbf{I} - \phi_0 (\sigma_0 - \sigma_2)^2 \times \begin{bmatrix} \tilde{D} & & \\ & \tilde{E} & \\ & & \tilde{F} \end{bmatrix}, \tag{43}$$

where

$$\begin{aligned} \tilde{D}^{-1} &= \phi_0(\sigma_2 - \sigma_0) + \phi_1 A_1 + \phi_2 B_2 + \phi_3 B_3, \\ \tilde{E}^{-1} &= \phi_0(\sigma_2 - \sigma_0) + \phi_2 A_2 + \phi_3 B_3 + \phi_1 B_1, \\ \tilde{F}^{-1} &= \phi_0(\sigma_2 - \sigma_0) + \phi_3 A_3 + \phi_1 B_1 + \phi_2 B_2. \end{aligned} \tag{44}$$

This result gives the *anisotropic Maxwell approximation* and is clearly a very minor variant of the results obtained earlier in (20) and (21) for the *isotropic Maxwell approximation*.

As will be discussed more fully later, the formula (20) can be used together with self-consistent estimates in certain types of sequential upscaling schemes. But some care in its use is required to avoid nonconvergence. In particular, since this formula is in fact a Maxwell approximation, it has some implicit assumptions about the smallness of the inclusion volume fractions, and also concerning the ratio of the background conductivity σ_0 to the inclusion conductivity. Care should be taken so that these assumptions are not violated within a complicated sequential estimation scheme.

In following subsubsections on *VTI or TTI symmetry* and *Three or more distinct fracture sets*, we discuss methods of treating nonisotropic overall conductivities using variants of these formulas when either two distinct or three distinct fracture sets are preesent, respectively. In subsubsection on *Some upscaling approximations to avoid*, we discuss an important special case of these formulas when $\sigma_0 \to \sigma_2$.

VTI or TTI symmetry

One special case important to consider has two orthogonal crack sets with the same porosity and the same aspect ratio, but the third set is different from these other two. Common examples of this situation are VTI or TTI symmetries. (a) For VTI (vertical transverse isotropy), two vertical sets of fractures are orthogonal to each other, but otherwise the same, having the same overall porosity and the same aspect ratio oblate spheroidal cracks. The third set of cracks in this case, which is assumed to consist of horizontal cracks then results in VTI symmetry, and will often have smaller porosity due to having smaller crack aspect ratios than the other two. This situation may be caused in part by the overburden pressure which will often tend to open the vertical cracks while at the same time tending to close any horizontal cracks. (b) For TTI (tilted transverse isotropy), the geometry is almost the same, with the axis of symmetry not being vertical, but rather tilted at some angle to vertical. Thus, tilted transverse isotropy can be modeled using exactly the same codes, etc., but at the last step, we will need to orient the results so the axis of symmetry is at the correct (tilted) angle to the vertical.

In the section **A Self-consistent Generalization of the Method for Higher Concentrations of Inclusions**, we proposed an approximate method for dealing with generally anisotropic systems. This approach involved averaging the effective constants via (26). This

method is expected to work well enough if the overall anisotropy is small in magnitude, deviating only somewhat from an isotropic system. If instead the system is very anisotropic, as it might well be in a VTI system (for example), then it will surely be worthwhile to consider other options. One obvious alternative is to pursue large scale first-principles code calculations. And such efforts could also be used then to provide additional validation to effective medium approaches, including the present ones. We might also attempt to work through a more general effective medium approach than the one presented herein, but such efforts must also remain in the category of future work for now.

We developed the main ideas in the preceding section on **Results for Resistive Inclusions** in order to prepare the way for what must be done to solve the present problem in a practical way. The key issue making this problem especially difficult is this: We do not have simple results at the present time for constructing good approximations to the overall behavior of conducting systems when the background medium is itself anisotropic, while at the same time the concentration of the fractures is sufficiently large that self-consistent methods are required. In some sense, we have already solved the noninteracting problem for mixed volume fractions of oriented conducting fractures in all three main directions. So it is only the interacting problem that we still need to solve; and the problem we encounter with this setup is that we do not have results yet for the quantitative effects inherent in imbedding an oriented conducting fracture in an already *anisotropic* background medium. And we really *must have such a result* to do the self-consistent calculation correctly. At some future time we may have such a result, but at the moment we must find some viable means of avoiding this step. So the question is what else can we do at present?

Suppose we have either two or three very different sets of fractures present. From the results of the section on **Results for Resistive Inclusions**, we know that each of these sets of fractures can be well characterized by a single independent variable which is the crack density $\rho_c = \phi/\alpha$. This idea works very well in general for the noninteraction approximation (Maxwell), but also for the self-consistent approximation (SC) when using values of ρ_c (< 2 or 3, for example) that are not too extreme. Now, let us suppose we can choose one of these oriented fracture sets having the smallest ρ_c, and call this value $\rho_c^{(1)}$. Then we can do a computation to determine what the effective isotropic conductivity would be for a system containing only this type of fracture in the background medium σ_0 in all three orientations. Next we can make use of the resulting isotropic conductivity σ_1^* as the new background value

for the other two fracture sets. But now we can also reduce the effects of the anisotropy due to these other two fracture sets by subtracting off the crack density value $\rho_c^{(1)} = \phi_1/\alpha_1$ (the meaning of the numbers $1, 2, 3$ in relation to the physical coordinate system is arbitrary here) from those of the other two conductivities $\rho_c^{(2)}$ and $\rho_c^{(3)}$. The results are:

$$0 \leq \Delta\rho_c^{(2)} = \frac{\phi_2}{\alpha_2} - \frac{\phi_1}{\alpha_1} = \frac{\Delta\phi_2}{\alpha_2} \implies \Delta\phi_2 = \phi_2 - \alpha_2\rho_c^{(1)}, \tag{45}$$

and

$$0 \leq \Delta\rho_c^{(3)} = \frac{\phi_3}{\alpha_3} - \frac{\phi_1}{\alpha_1} = \frac{\Delta\phi_3}{\alpha_3} \implies \Delta\phi_3 = \phi_3 - \alpha_3\rho_c^{(1)}, \tag{46}$$

which define the new values of effective porosities $\Delta\phi_2$ and $\Delta\phi_3$ that we will need to use in the final self-consistency calculation. Equations (45) and (46) also make clear why it is important to choose the smallest value ρ_c as the one to use for the first step, since it is not at all a good idea to use negative porosity changes $\Delta\phi_2$ and $\Delta\phi_3$ in the self-consistency method. Also, the equations (45) and (46) guarantee nonnegative Δ's if a correct ρ_c (minimum) value is used in the isotropic background calculation.

In concept, we expect this method should work well because we are assuming that all three fracture sets contain the same pore-fluid, thus having the same fluid conductivity σ_2. The point of this exercise is that the rock conductivity background value σ_0 is typically many orders of magnitude smaller than the conductivity σ_2 of the fluid in all the fractures. By moving the contribution of the isotropic background material from that of the host conductivity value σ_0 (which is very small) to that of the effective conductivity value σ_1^* (which is much closer to the expected final result), we should have greatly reduced the need for the self-consistent approximation (thus making the final SC calculation easier/quicker to converge). This approach may have also largely eliminated the need for some other previously discussed technical results (*i.e.*, such as embedding anisotropic inclusions in an anisotropic background, as mentioned previously) that have not yet been treated. (This issue can only be properly resolved by carrying through the harder anisotropic background calculation. Such work is currently at the planning stage, but beyond the scope of the present paper.)

Three or more distinct fracture sets

The method developed in the previous subsection for cases having only two sets of distinct types of fracture sets is clearly general enough to be applied to systems of three or more distinct fracture sets of the types that we have been discussing. The only general concerns with this approach are: (1) that the fluid in all the fracture sets needs to be same (if this is not true then further generalization will be required, but this is not being considered in the present work), and (2) that all the crack densities should not be much higher than about 3. The saturating fluids must have the same conductivity in order for the subtractions in (45) and (46) to make sense in this logical framework. And the crack densities should not be much higher than about 3, because of the results shown in Figure 5, where the effects of cracks for the smaller values of $\rho_c < 1$ are seen to depend effectively only on crack density ρ_c, as was anticipated.

Some upscaling approximations to avoid, and other potential problems with convergence of the method

As will be discussed in more detail a little later in the paper, it is sometimes useful to apply the formulas presented to complicated systems sequentially, arriving at intermediate upscaling results that can then be used to simplify the problem, and possibly improve convergence of these methods in difficult modeling scenarios. It is important however to recognize that there are limitations to such methods, and one of these limitations will be pointed out now.

We have been attempting to model systems having high contrast between the insulating host medium and the highly conducting inclusions. Thus, the model implicitly assumes that $\sigma_0 << \sigma_2$. If we try to apply the methods sequentially so that the true background value σ_0 is replaced by some effective value — say σ^{**}, it is important to notice what happens to the results contained in (40)–(44) in such cases. As the value $\sigma_0 \simeq \sigma^{**} \to \sigma_2$, we find that the leading terms of the form $1/(\sigma_2 - \sigma_0)$ start to dominate the secondary terms for both A_j and B_j. So we find $A_j \to B_j \to (\sigma_2 - \sigma_0)$, for all $j = 1, 2, 3$. Thus, all the expressions in (44) also tend towards the value $(\sigma_2 - \sigma_0)$. In this limit, we then find that (20) approaches

the result:

$$\mathbf{\Sigma}_e \to [(1-\phi_0)\sigma_2 + \phi_0\sigma_0]\,\mathbf{I}, \tag{47}$$

which is exactly the Wiener upper bound for this problem. Since this bound is the highest value we ever need to consider, and since – under the circumstances we are focusing attention upon in which background value σ_0 has been replaced by an effective value as discussed in subsubsections 8.1.1 and 8.1.2 — the actual value of σ_0 has presumably been replaced by some larger approximate value σ^{**}, this limiting value is clearly an undesirable one. So some caution is appropriate when attempting to use these upscaling methods sequentially.

Since the self-consistent effective medium method is itself an inherently sequential-upscaling method, it is important to keep these limitations in mind when applying it to a wide range of problems. In particular, the user should be aware that it is possible that the self-consistent method presented here will in some cases fail to converge. One mode of failure the authors have observed normally arises when applying the isotropic averaging approximation in a situation where the overall system is highly anisotropic. Then, the method updates the average background to a higher value at each step, and tries to fit this average (the one from the previous step). Failing to do so at each step causes the scheme to ratchet upward slightly at each iteration step, but never truly converges until it achieves such a high value of overall conductivity that it is bounded above by the rigorous bounds. But such results can add nothing to our understanding of these systems since we could just as easily (or more easily) have used those bounds in the first place, skipping the iteration steps that lead us back to these results through this complicated process. This observed failure mode is not universal, but nevertheless it is sufficiently common that the present warning should be duely noted. It is anticipated that this problem might appear whenever the system being studied displays highly anisotropic behavior. Fortunately, experience shows that moderate anisotropy seems to be tolerated well by all the methods discussed here.

Vertical fractures having an oblique angle between them

Another issue concerns how the results change if any two of the three sets of fractures considered are not orthogonal, as has been previously assumed. The most interesting case is probably the one in which the vertical fractures being considered are not all either exactly parallel or exactly perpendicular to each other. We will term such possibilities the "oblique

cases" for vertical fractures. If there is only one pertinent angle between the fractures, or just a small number of closely distributed angles, we can presumably decompose the electrical conduction behavior into two effectively orthogonal components. For any angle θ between these vertical fracture sets then should be a well-defined (*i.e.*, average) half-angle $\equiv \theta/2$. This computed direction splits the difference between the two fracture sets, and presumably is the direction of highest conductivity parallel to the earth's surface, while the vertical conductivity is still higher since both fracture sets are still contributing in parallel in the vertical direction.

So nonorthogonal vertical fracture sets should have highest conductivity in the vertical direction, and lowest in the direction perpendicular to the smallest half-angle between them. The third and intermediate conductivity value will be parallel to the half-angle between these fractures. Such combined fracture sets might therefore appear phenomenologically to act on the average as a single fracture set. Many diverse sets of angles among the vertical fractures might also create an essentially isotropic distribution of conductivity in planes parallel to the surface. Analysis of all these possible scenarios is not difficult if care is taken to account for the great diversity of conduction paths that is possible, as well as the very well understood properties of series and parallel circuit analysis for conducting arrays.

Modifications resulting from possible violations of prior assumptions

Clearly other violations of the present assumptions are also possible. For example, the fluids in the fractures might not all be exactly the same, and therefore the conductivities that are introduced into the system by these locally differing conductivities would need to be taken into account as well. These issues are not addressed here specifically, but the formulation presented is sufficiently general that it could be modified easily with only a little effort needed to account for such diversity (for example, via mathematical distribution functions) in the field behavior.

WORKED EXAMPLE FOR THREE DISTINCT FRACTURE SETS

As a way of summarizing what we have learned, we will now work through one example of how these ideas can be put into practice when there are three differently oriented fractures,

while the three sets also have different fracture aspect ratios and different volume fractions (porosities).

The model we consider is this: Fracture set 1 has porosity $\phi_1 = 0.089$; fracture set 2 has porosity $\phi_2 = 0.111$; fracture set 3 has porosity $\phi_3 = 0.133$. Each of these fracture sets individually has uniform aspect ratio, taken from the three choices: $\alpha_1 = 0.05$, $\alpha_2 = 0.10$, $\alpha_3 = 0.15$. The corresponding crack densities are: $\rho_c^{(1)} = 0.89$, $\rho_c^{(2)} = 2.22$, and $\rho_c^{(3)} = 1.33$. Of these three sets, the first one has the lowest crack density, which is $0.89 < 1.0$. Because of the results shown in Figures 4 and 5, we expect the method being employed to work best when the lowest crack density falls below $\rho_c = 1.0$, but not too far below this value, since we want to include as much of the porosity as possible into the effective isotropic background material being computed.

Now we can construct this model – the one that will become the new background for our final Maxwell calculation – by taking the fracture set with the lowest crack density, and doing a self-consistent calculation assuming this fracture set, and two others having the same porosity and the same aspect ratio (these fractures are in fact totally artificial, but are being used to replace the effects of some subsets of the other two real sets of fractures, both of which have higher crack density than the first one), but mutually orthogonal orientations. The resulting model is that of an isotropic system having uniform crack density ($\rho_c \equiv \phi/\alpha$), aspect ratios ($\alpha$), and porosities ($\phi$) everywhere. And this is the ideal circumstance for performing the self-consistent calculation. We have already described this procedure before and so do not need to do so again here. We find that, when the host and inclusion conductivities are once again given by $\sigma_0 = 0.001$ and $\sigma_2 = 5.0$ S·m^{-1}, that the result of this calculation is a uniform, isotropic conductivity value of $\sigma^* = 0.68565$ S·m^{-1}.

Next, because the actual problem we are trying to solve also contains two other fracture sets, we need to incorporate the effects of these remaining two sets into the overall conductivity using a Maxwell approximation. To enable this process, we need to reduce the effective porosity of the other two sets by taking advantage of the crack density concept. We find that $\Delta\phi_2 = 0.111 - 0.89 \times 0.05 = 0.081333$, and $\Delta\phi_3 = 0.133 - 0.89 \times 0.10 = 0.073667$. Then, we perform a Maxwell calculation, assuming now that $\Delta\phi_1 \equiv 0.0$ (since this part has already been incorporated into the host medium), the other two $\Delta\phi$'s were just given, while the host medum now has $\sigma_0 = 0.68565$, and the fluid-inclusion conductivity is the same value as before: $\sigma_2 = 5.0$. We then do the simple one-step Maxwell calculation, and the

result that we find is:

$$\mathbf{\Sigma}^* = \begin{pmatrix} 1.2106 & & \\ & 0.9592 & \\ & & 1.0473 \end{pmatrix}. \tag{48}$$

These values are all higher than the background value of 0.6857 and the differences are approximately proportional (respectively) to $\Delta\phi_2 + \Delta\phi_3$, $\Delta\phi_3$, and $\Delta\phi_2$, as would be expected from the analysis resulting in (23). We do NOT expect these results to conform perfectly with the form of (23), because that result was for systems having uniform crack aspect ratios (*i.e.*, Q was constant).

In the present calculation, crack density, crack aspect ratio, porosity, effective porosity, etc., are all different from one fracture set to the others, and there are no obvious further simplifications that could be made to the model than the main one we already introduced based on determining a reasonable estimate of an isotropic background crack density and a corresponding isotropic conductivity model associated with that crack density. We believe that, at the present time [until these self-consistent methods have been generalized for application to anisotropic systems — *i.e.*, based on work such as that of Carslaw and Jaeger (1959), Rocha and Acrivos (1973a,b), and Chen (1976)], this type of estimate is one of the better choices available to us that can be obtained relatively easily using these effective medium methods.

DISCUSSION AND CONCLUSIONS

When attempting to model the behavior of earth materials containing fractures, there are various models in common use. One frequent choice that we have not pursued here considers layered materials. In such a model, a fracture can be treated as its own layer. The main advantage of this approach is the simplicity of the averaging method (layered models are very easy to quantify, especially for conductivity applications); while the main disadvantage is that this geometry can be too special and therefore fairly unrealistic, especially if we also want to model elastic behavior at the same time as the electrical conductivity, or fluid-flow permeability. The treated model results have also been compared by the authors to results of layered models, and the results were quantitatively very similar; but we have chosen not to show these comparisons here to help limit the length of the paper. At the very least,

such layered models should be generalized so as to treat them as being poroelastic in their mechanical aspects (Berryman, 2011).

We have chosen to treat the fractures here as being highly electrically conductive (or possibly resistive) ellipsoidal inclusions. This model is surely also subject to criticism, since it is quite unlikely that actual fractures are of precisely this shape. On the whole, the presented model appears to provide a very reasonable aspproximate description of complicated anisotropic electrical behavior in many cases. And we have shown explicitly that the concept of crack density $\rho_c \equiv \phi/\alpha$ is one very useful tool for relating systems having quantitatively similar behavior, even though the true microgeometry may be very different from that of simple ellipsoids.

Eq. (10) is a general formula for the effective electrical conductivity $\mathbf{\Sigma}_e$ of the composite material having various ellipsoidal inclusions of any given orientation. That formula is implicit as written, since the desired quantity $\mathbf{\Sigma}_e$ appears on both sides of the equation. This equation can be solved numerically either by iteration, or by a numerical inversion of the matrix:

$$\left[\mathbf{I} + \frac{1}{\phi_0}\sum_j \phi_j \mathbf{R}^{(j0)}\right]. \tag{49}$$

For most cases studied in detail here, this matrix (49) was actually diagonal, and therefore trivial to invert. But for arbitrary orientations of these ellipsoids in space, the matrix becomes full and, therefore, a numerical inversion procedure (for a 3×3 matrix) will be required in general.

We introduced self-consistent methods for overall isotropic systems and also for anisotropic systems. In both cases, these models have been successfully treated for highly conducting fluid (such as ocean brine) inclusions in the form of saturated fractures (oblate spheroids) in a more poorly conducting host medium (earth or earth plus poorly conducting fluid inclusions). Application of the same methods to cases having more resistive inclusions than the host medium itself were found to be problematic for the self-consistent method, but were nevertheless handled quite readily by the Maxwell approximation approach. The Maxwell approximation is always valid for either more conductive or more resistive inclusions as long as the volume fraction of the inclusions is not too large. Therefore, Maxwell approximation should probably not be used for porosities much above $\phi = 0.1$. The SC approximation seems to be reliable for conductive inclusions up to about $\phi = 0.20$. The

convergence of the SC iteration scheme was found to be dependent on crack density $\rho_c = \phi/\alpha$, and we generally obtain that, for $\rho_c \geq 0.2$, the self-consistent scheme can have convergence problems. When this happens, it might be appropriate to switch to the Maxwell approximation, but this method is limited as well, since it does not take interactions between inclusions for general shapes properly into account.

Within the limitations already discussed, we have found that the recommended effective medium methods do converge to reasonable models for these systems, *e.g.*, for models that typically satisfy rigorous bounds such as Wiener (1912) and Hashin-Shtrikman (1962) bounds. There are currently some limitations of these methods that can likely be eliminated if some more technical results (Rocha and Acrivos, 1973a,b; Chen 1976) were to be implemented, so that the background (host) medium could be treated consistently as anisotropic itself. Developing both formulas and effective medium theories (such as an improved self-consistent method) in order to quantify the effect of adding one or many conducting ellipsoids of arbitrary orientation(s) to an *anisotropic* conducting host material is therefore an important goal for our future research – especially when aimed at potential improvements to our modeling capabilities for higher porosities, higher crack densities, and highly resistive inclusions.

Acknowledgments

The authors thank David Alumbaugh for his efforts in checking all the code calculations used in the examples of this paper. Work of JGB performed under the auspices of the U.S. Department of Energy, at the Lawrence Berkeley National Laboratory under Contract No. DE-AC02-05CH11231. Support of the project "Electrical Conductivity of Fluid-Filled Fractures" – of which this paper is the main output – was provided by a grant from the Chevron Energy Technology Company. Some additional support was provided by the Geosciences Research Program of the DOE Office of Basic Energy Sciences, Division of Chemical Sciences, Geosciences, and Biosciences during the completion, review, and publication phases of the work. All support of this research is hereby gratefully acknowledged.

REFERENCES

Avellaneda M., 1987, Iterated homogenization, differential effective medium theory, and applications, *Communications in Pure and Applied Mathematics* **40**, 5527–554.

Aydin A. and Berryman J. G., 2010, Analysis of the growth of strike-slip faults using effective medium theory, *Journal of Structural Geology* **32**, 1629–1642.

Berge P. A., Berryman J. G. and B. P. Bonner, 1993, Influence of microstructure on rock elastic properties, *Geophysical Research Letters* **20**, 2619–2622.

Berryman, J. G., 1985, Bounds on fluid permeability for viscous flow through porous media, *Journal of Chemical Physics* **82**, 1459–1467.

Berryman J. G., 1995, Mixture theories for rock properties, in *Rock Physics and Phase Relations: A Handbook of Physical Constants*, ed. T. J. Ahrens, American Geophysical Union, Washington, D.C., pp. 205–228.

Berryman J. G., 2007, Seismic waves in rocks with fluids and fractures, *Geophysical Journal International* **171**, 954–974.

Berryman J. G., 2008, Elastic and transport properties in polycrystals of cracked grains: Cross-property relations and microstructure, *International Journal of Engineering Science* **46**, 500–512.

Berryman, J. G., 2009, Aligned vertical fractures, HTI reservoir symmetry and Thomsen seismic anisotropy parameters for polar media, *Geophysical Prospecting* **57**, 193–208.

Berryman, J. G., 2010, Pore-fluid effects on seismic waves in vertically fractured earth with orthotropic symmetry, *Geophysics* **75**, T185–T200.

Berryman J. G., 2011, Mechanics of layered anisotropic poroelastic media with applications to effective stress for fluid permeability, *International Journal of Engineering Science* **49**, 122–139.

Berryman J. G. and Berge P. A., 1996, Critique of explicit schemes for estimating elastic properties of multiphase components, *Mechanics of Materials* **22**, 149–164.

Berryman J. G. and Grechka V., 2006, Random polycrystals of grains containing cracks: Model of quasistatic elastic behavior for fractured systems, *Journal of Applied Physics* **100**, 113527.

Berryman J.G. and Milton G. W., 1985, Normalization constraint for variational bounds on fluid permeability, *Journal of Chemical Physics* **83**, 754–760.

Berryman J. G., Pride S. R. and Wang, H. F., 2002, A differential scheme for elastic properties of rocks with dry or saturated cracks, *Geophysical Journal International* **151**, 597–611.

Bristow J. R., 1960, Microcracks, and the static and dynamic elastic constants of annealed and heavily cold-worked metals, *British Journal of Applied Physics* **11**, 81–85.

Brown W. F., Jr., 1955, Solid mixture permittivities, *Journal of Chemical Physics* **23**, 1514–1517.

Budiansky, B., and O'Connell R. J., 1976, Elastic moduli of a cracked solid, *Int. J. Solids and Structures* **12**, 81–97.

Carslaw H. S. and Jaeger J. C., 1959, *Conduction of Heat in Solids*, Oxford University Press, Oxford, UK, p. 427.

Chen H.-S., 1976, Conduction through an anisotropic suspension of aligned ellipsoids, *Letters in Heat and Mass Transfer* **3**, 449–456.

Cherkaev A., 2000, *Variational Methods for Structural Optimization*, Springer-Verlag, New York, Chapters II and IV.

Dey A. and Morrison H. F., 1979, Resistivity modeling for arbitrary shaped three-dimensional structures, *Geophysics* **44**, 753–780.

Fokker P. A., 2001, General anisotropic effective medium theory for effective permeability of heterogeneous reservoirs, *Transport in Porous Media* **44**, 205–218.

Grechka V., 2005, Penny-shaped fractures revisited, *Stud. Geophys. Geod.* **49**, 365–381.

Grechka V. and Kachanov M., 2006a, Effective elasticity of rocks with closely spaced and intersecting cracks, *Geophysics* **71**, D85-D91.

Grechka V. and Kachanov M., 2006b, Seismic characterization of multiple fracture sets: Does orthoropy suffice?, *Geophysics* **71**, D93-D105.

Hashin Z. and Shtrikman S., 1962, A variational approach to the theory of the effective magnetic permeability of multiphase materials, *Journal of Applied Physics* **33**, 3125–3131.

Herrick D. C. and Kennedy W. D., 1994, Electrical efficiency – A pore geometric theory for interpreting the electrical properties of reservoir rocks, *Geophysics* **59**, 918–927.

Hoversten G. M., Cassassuce F., Gasperikova E., Newman G. A., Chen J. S., Rubin Y., Hou Z. S. and Vasco D., 2006a, Direct reservoir parameter estimation using joint inversion of marine seismic AVA and CSEM data, *Geophysics* **71**, C1–C13.

Hoversten G. M., Newman G. A., Geier N. and Flanagan G., 2006b, 3D modeling of a deepwater EM exploration survey, *Geophysics* **71**, G239–G248.

Hudson, J. A., 1981, Wave speeds and attenuation of elastic waves in material containing cracks, *Geophys. J. Roy. Astron. Soc.* **64**, 133–150.

LaBrecque, D. J., Miletto, M., Daily, W., Ramirez, A., and Owen, E., 1996, The effects of noise on Occam's inversion of resistivity tomography data, *Geophysics* **61**, 538–548.

Long, J. C. S., Remer, J. S., Wilson, C. R., and Witherspoon, P. A., 1982, Porous media equivalents for networks of discontinuous fractures, *Water Resources research* **18**, 645–658.

Mavko G., Mukerji T., and Dvorkin J., 2009, *The Rock Physics Handbook (Second Edition)*, Cambridge University Press, Cambridge, UK.

Milton G. W., 1985, The coherent potential approximation is a realizable effective medium scheme, *Communications in Mathematical Physics* **99**, 463–500.

Milton G. W., 2002, *The Theory of Composites*, Cambridge University Press, Cambridge, UK, pp. 115, 192–195.

Milton G. W., 2012, Universal bounds on the electrical and elastic response of two-phase bodies and their application to bounding the volume fraction from boundary measurements, *Journal of the Mechanics and Physics of Solids* **60**, 139–155.

Newman G. A., Commer M. and Carazzone J. J., 2010, Imaging CSEM data in the presence of electrical anisotropy, *Geophysics* **75**, F51–F61.

Norris A. N., 1985, A differential scheme for the effective moduli of composites, *Mechanics of Materials* **4**, 1–16.

Norris A. N., P. Sheng and A. J. Callegari, 1985, Effective medium theories for two-phase dielectric media, *Journal of Applied Physics* **57**, 1990–1996.

O'Connell R. J. and Budiansky B., 1977, Viscoelastic properties of fluid-saturated cracked solids, *Journal of Geophysical Research* **82**, 5719–5736.

Renard Ph. and de Marsily G., 1997, Calculating equivalent permeability: A review, *Advances in Water Resources* **20**, 253–278.

Rocha A. and Acrivos A., 1973a, On the effective thermal conductivity of dilute dispersions: General theory for inclusions of arbitrary shape, *Quarterly Journal of Mechancis and Applied Mathematics* **26** (2), 217–233.

Rocha A. and Acrivos A., 1973b, On the effective thermal conductivity of dilute dispersions: Highly conducting inclusions of arbitrary shape, *Quarterly Journal of Mechanics and Applied Mathematics* **26** (4), 441–455.

Sen P. N., C. Scala and M. H. Cohen, 1981, A self-similar model for sedimentary rocks with

application to the dielectric constant of fused glass beads, *Geophysics* **46**, 781–795.

Shafiro B. and Kachanov M., 2000, Anisotropic effective conductivity of materials with nonrandomly oriented inclusions of diverse ellipsoidal shapes, *Journal of Applied Physics* **87** (11), 8561–8569.

Stratton J. A., 2007, *Electromagnetic Theory*, IEEE Press, Wiley-Interscience, Hoboken, New Jersey.

Stroud D., 1975, Generalized effective-medium approach to the conductivity of an inhomogeneous material, *Physical Review B* **12**, 3368–3373.

Torquato S., 2002, *Random Heterogeneous Materials: Microstructure and Macroscopic Properties*, Springer, New York.

Wiener O., 1912, Die Theories des Mischkörpers für das Feld des stationären Strömung, *Abh. Math.-Physichen Klasse Königl. Sächsh. Gesel. Wissen.* **32**, 509–604.

Witherspoon, P. A., Wang, J. S. Y., Imai, K., and Gale, J. E., 1980, Validity of the cubic law for fluid flow in a deformable rock fracture. *Water Resources Research* **16**, 1016–1024.

Zhou B., Greenhalgh M., and Greenhalgh S. A., 2009, 2.5-D/3-D Resistivity modelling in anisotropic media using Gaussian quadrature grids, *Geophysical Journal International* **176**, 63–80.

Zhou B. and Greenhalgh S. A., 2001, Finite element three-dimensional direct current resistivity modeling: Accuracy and efficiency considerations, *Geophysical Journal International* **145**, 676–688.

Zimmerman R. W., 1991, *Compressibility of Sandstones*, Elsevier, New York, pp. 113-127.

APPENDIX: CALCULATING THE DEPOLARIZATION A-MATRIX FOR OBLATE SPHEROIDS

[Note: In the following analysis, we are using Stratton's definitions of the spheroid dimensions (Stratton, 2007), but Torquato's choice of normalization of the matrix elements of the depolarization matrix $\mathbf{A}$ (Torquato, 2002).]

When a uniform electric field $\mathbf{E}_0$ is applied to a polarizable system, the local polarization field $\mathbf{P}$ and the electrical intensity field $\mathbf{E}$ are given by $\mathbf{P} = \mathbf{M} \cdot \mathbf{E}_0$ and $\mathbf{E} = \mathbf{R} \cdot \mathbf{E}_0$. For background/host conductivity σ_0 and inclusion conductivity σ_2, the inclusion-shape dependent second-order tensors $\mathbf{M}$ and $\mathbf{R}$ are given then by $\mathbf{M} = (\sigma_2 - \sigma_0)\mathbf{R}$, and $\mathbf{R} =$

$[\mathbf{I} + \mathbf{A}(\sigma_2 - \sigma_0)/\sigma_0]^{-1}$, with $\mathbf{I}$ being the 3×3 identity matrix. $\mathbf{A}$ is a symmetric (and here limited to diagonal) tensor of depolarization factors, such that the components satisfy $0 \leq A_i \leq 1$, for $i = 1, 2, 3$ in 3D.

Stratton (p. 214) shows that one pertinent elliptic integral for oblate spheroids is

$$\frac{2}{a^2 c} A_3 \equiv \int_0^\infty \frac{ds}{(s + c^2) R(s)}, \tag{50}$$

where in general for ellipsoids having semi-axes a, b, c, we have

$$R(s) = \sqrt{(s + a^2)(s + b^2)(s + c^2)}. \tag{51}$$

For an oblate spheroid having two large dimensions of length $a = b$, and one short dimension of length c, the result obtained by Stratton is:

$$\frac{2}{a^2 c} A_3 = \int_0^\infty \frac{ds}{(s + a^2)(s + c^2)^{3/2}} = \frac{2}{(a^2 - c^2)^{3/2}} \left[\frac{\sqrt{a^2 - c^2}}{c} - \arctan\left(\frac{\sqrt{a^2 - c^2}}{c} \right) \right], \tag{52}$$

Torquato (p. 442) gives :

$$A_1 = Q = \frac{1}{2} \left\{ 1 + \frac{1}{(c/a)^2 - 1} \left[1 - \frac{\arctan(\sqrt{(a/c)^2 - 1})}{\sqrt{(a/c)^2 - 1}} \right] \right\}, \tag{53}$$

where the depolarization matrix

$$\mathbf{A} = \begin{bmatrix} Q & & \\ & Q & \\ & & 1 - 2Q \end{bmatrix} \tag{54}$$

is diagonal in this representation, which is aligned with the principal axes of the oblate spheroid.

It follows that Torquato's result satisfies $A_3 = 1 - 2Q = 1 - 2A_1 = 1 - 2A_2$, and also that

$$\frac{2}{a^2 c} A_3 = \frac{2}{(a^2 - c^2)^{3/2}} \left[\frac{\sqrt{a^2 - c^2}}{c} - \arctan\left(\frac{\sqrt{a^2 - c^2}}{c} \right) \right], \tag{55}$$

the right hand side of which is exactly Stratton's result [as shown in (52)] for his choice of the normalization of $\mathbf{A}$.

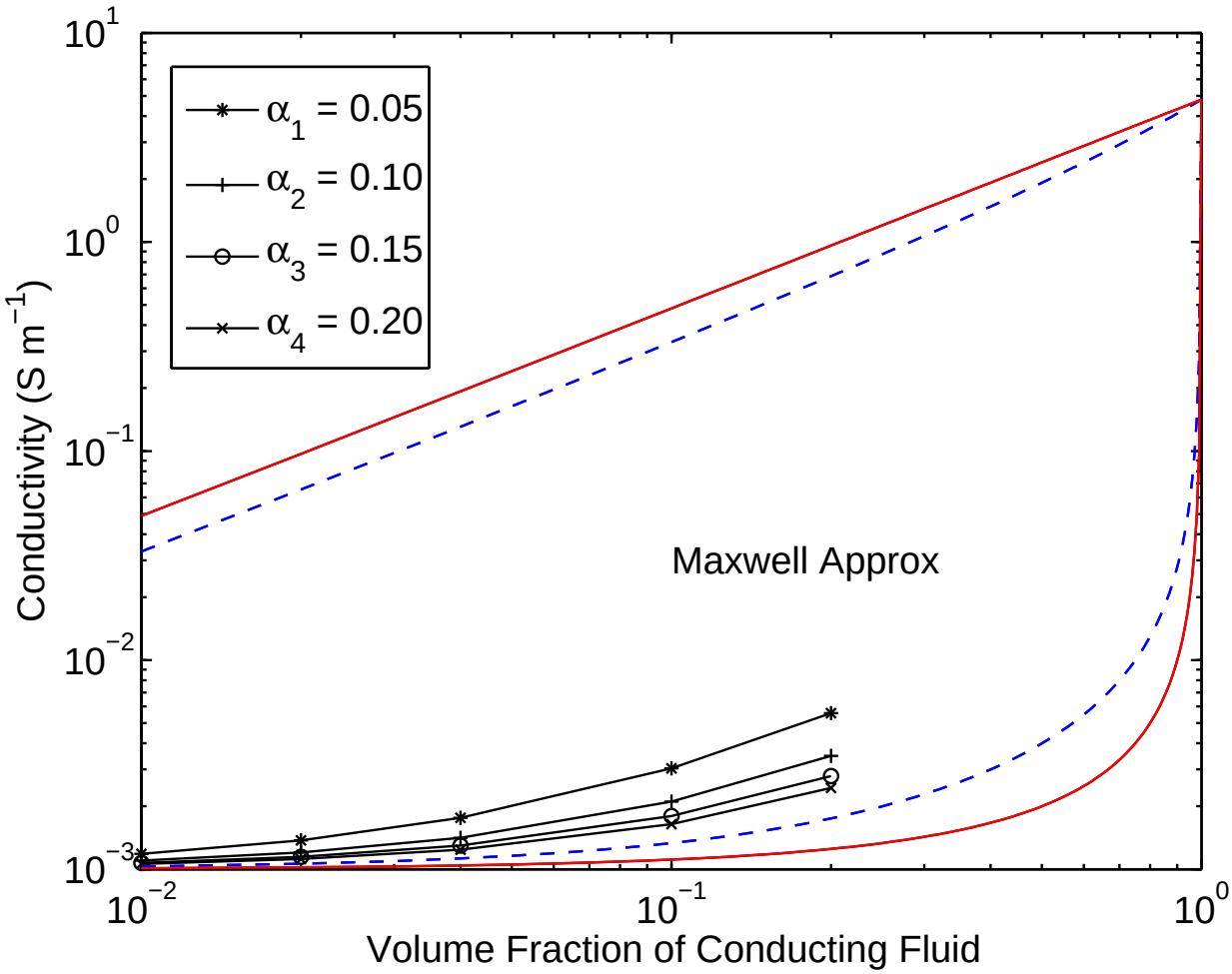

FIG. 1: Log-log plot of effective conductivity estimators. Black curves correspond to the Maxwell approximation for four choices of the fracture aspect ratio: $\alpha_1 = 0.05$, $\alpha_2 = 0.10$, $\alpha_3 = 0.15$, and $\alpha_4 = 0.20$. Volume fractions considered are $\phi_2 = 0.01$, 0.02, 0.04, 0.10, and 0.20. Red lines are the upper and lower Wiener bounds on conductivity. The dashed blue lines are the upper and lower Hashin-Shtrikman bounds. The host medium is assumed to be a basalt (or dry sand) having conductivity $\sigma_0 \simeq 0.001$ S$\cdot$ m^{-1}. The conducting brine inside the fractures is assumed to have $\sigma_2 \simeq 4.8$ S$\cdot$ m^{-1}.

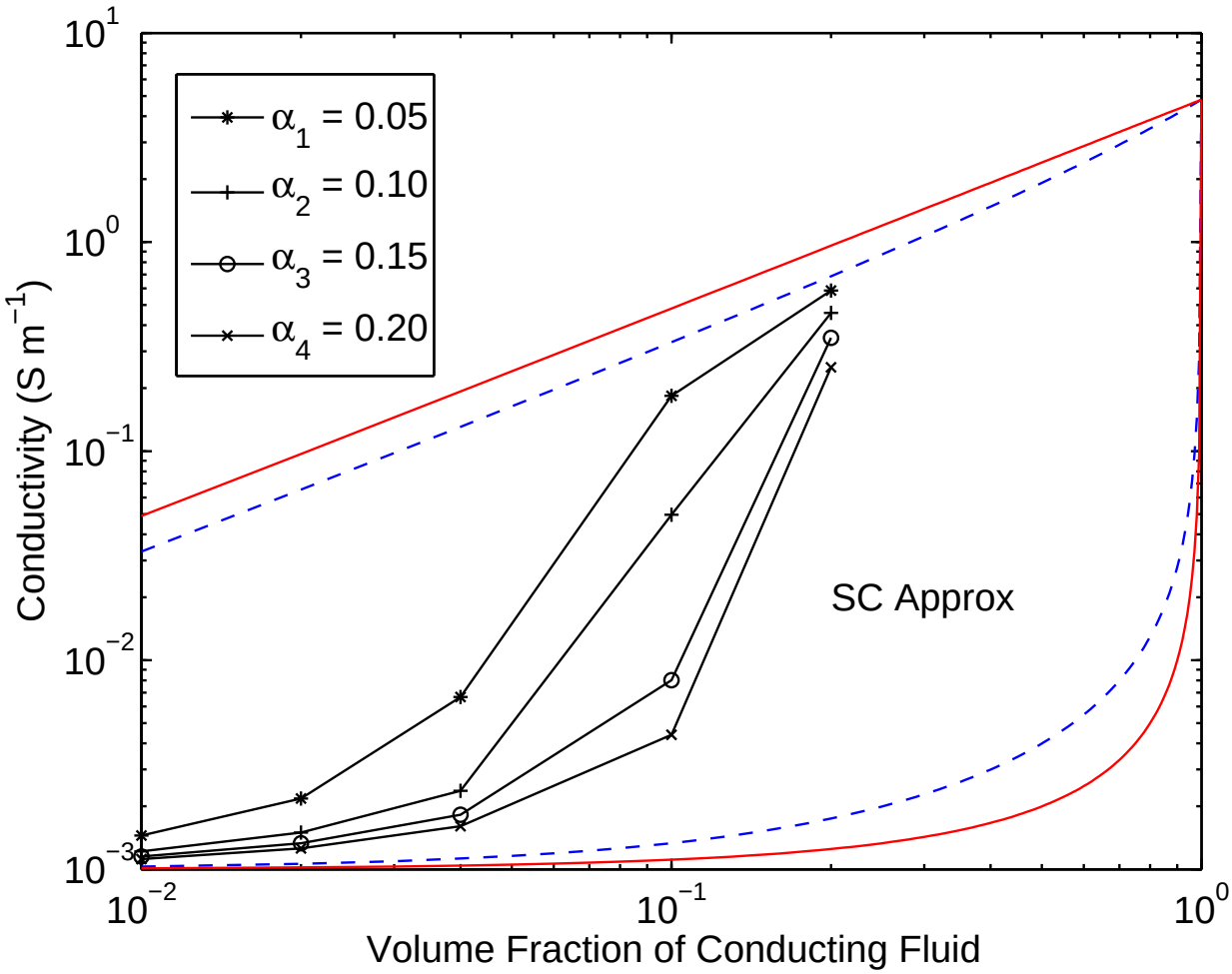

FIG. 2: Log-log plot of effective conductivity estimators. Black curves correspond to the self-consistent (SC) approximation for the same four choices (those also considered in Fig. 1) of the fracture aspect ratio: $\alpha_1 = 0.05$, $\alpha_2 = 0.10$, $\alpha_3 = 0.15$, and $\alpha_4 = 0.20$. Volume fractions considered are $\phi_2 = 0.01$, 0.02, 0.04, 0.10, and 0.20. Red lines are the Wiener bounds on conductivity; blue dashed lines are the corresponding Hashin-Shtrikman upper and lower bounds. Input conductivities for host and inclusion are the same as in Figure 1.

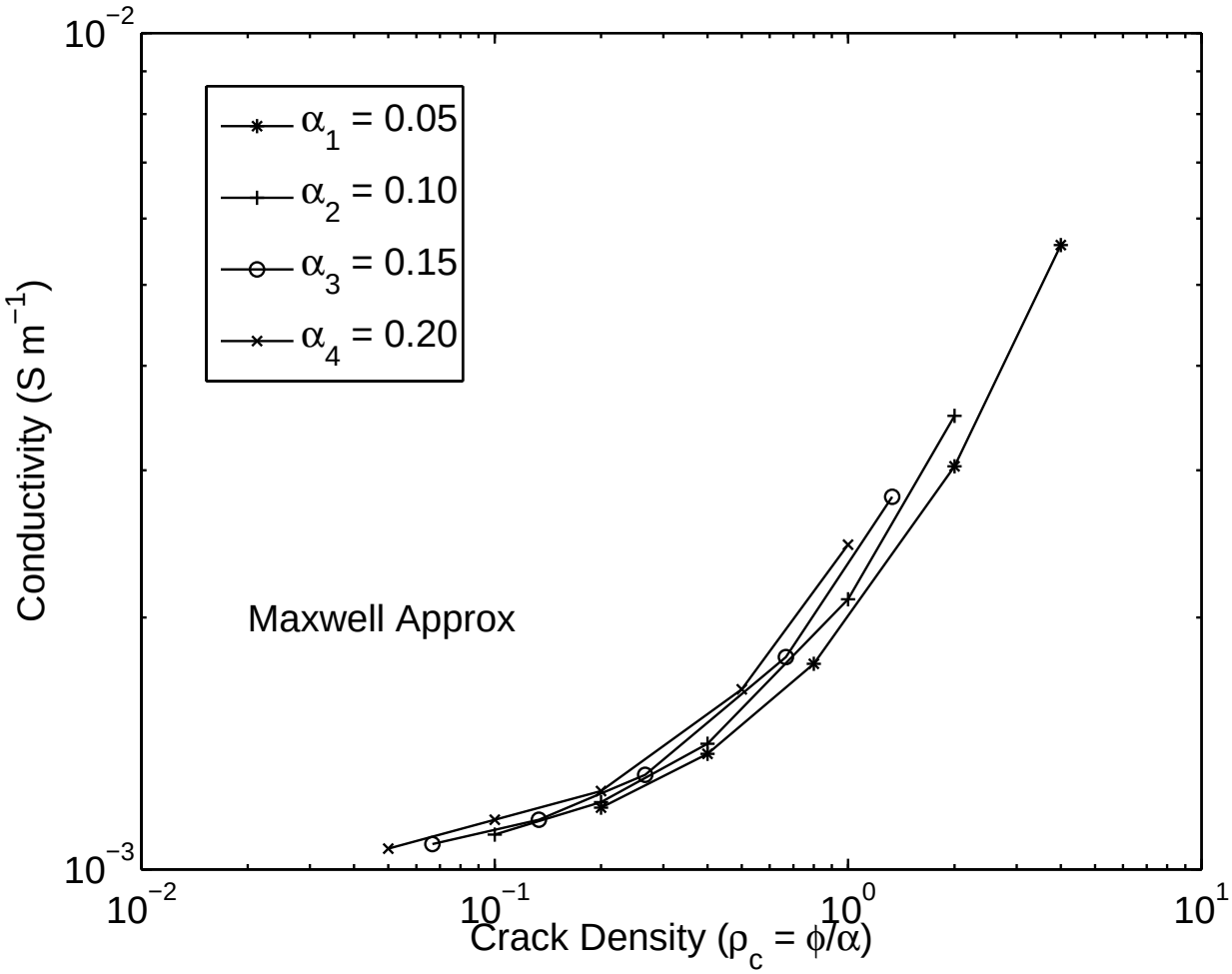

FIG. 3: Log-log plot of effective conductivity estimators versus crack density (see the section on **Crack Density Analysis**). All curves correspond to the Maxwell approximation for four choices of the fracture aspect ratio: $\alpha_1 = 0.05$, $\alpha_2 = 0.10$, $\alpha_3 = 0.15$, and $\alpha_4 = 0.20$. Volume fractions are considered from $\phi_2 = 0.01$ to 0.20. Crack density is defined as $\rho_c \equiv \phi/\alpha$. To appreciate the importance of plotting the results versus crack density, these curves should also be compared to those in Figure 1. Note that these results all apparently fall close to a nearly universal curve for the cases considered here. This apparent universality is due in part to the fact that the Maxwell approximation does not take interactions between inclusions actively into account. The bounds shown in Figs. 1 and 2 do not depend on aspect ratio and, therefore, are not pertinent for these comparisons.

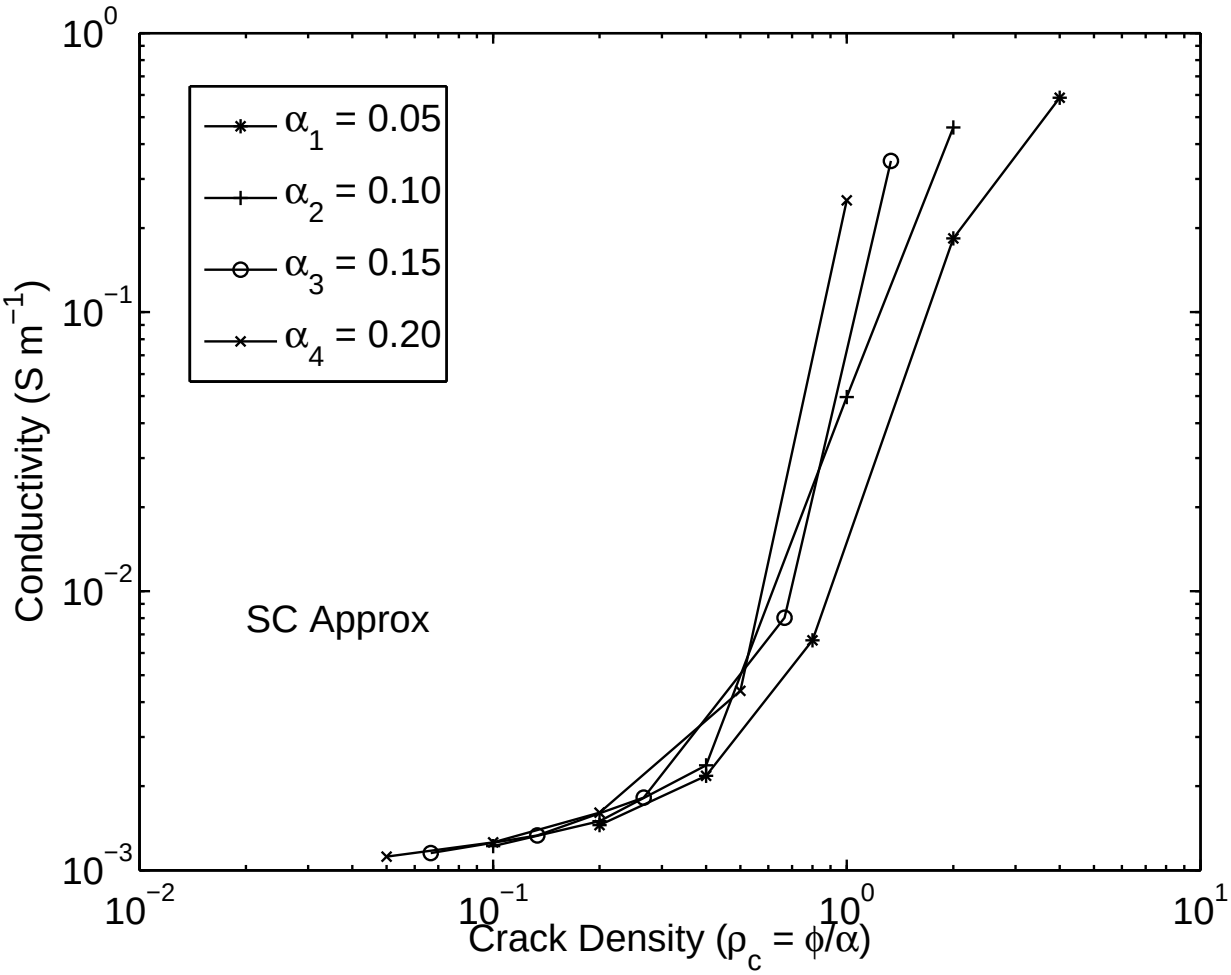

FIG. 4: Log-log plot of effective conductivity estimators. Black curves correspond to the self-consistent (SC) approximation for the same four choices (those considered in Fig. 2) of the fracture aspect ratio: $\alpha_1 = 0.05$, $\alpha_2 = 0.10$, $\alpha_3 = 0.15$, and $\alpha_4 = 0.20$. Volume fractions considered range from $\phi_2 = 0.01$ to 0.20. Crack density is defined here as $\rho_c \equiv \phi/\alpha$. Note that, for all crack aspect ratios α_1, α_2, α_3, and α_4, these computed results apparently lie on a nearly universal curve for small $\rho_c < 0.2$. The results for larger values of ρ_c clearly do not necessarily lie on such a universal curve. To appreciate the value of plotting these curves versus crack density more fully, the results should also be compared to those in Figure 3. The Wiener and Hashin-Shtrikman bounds actually do not depend on fracture aspect ratio, and so are not pertinent for comparisons here.

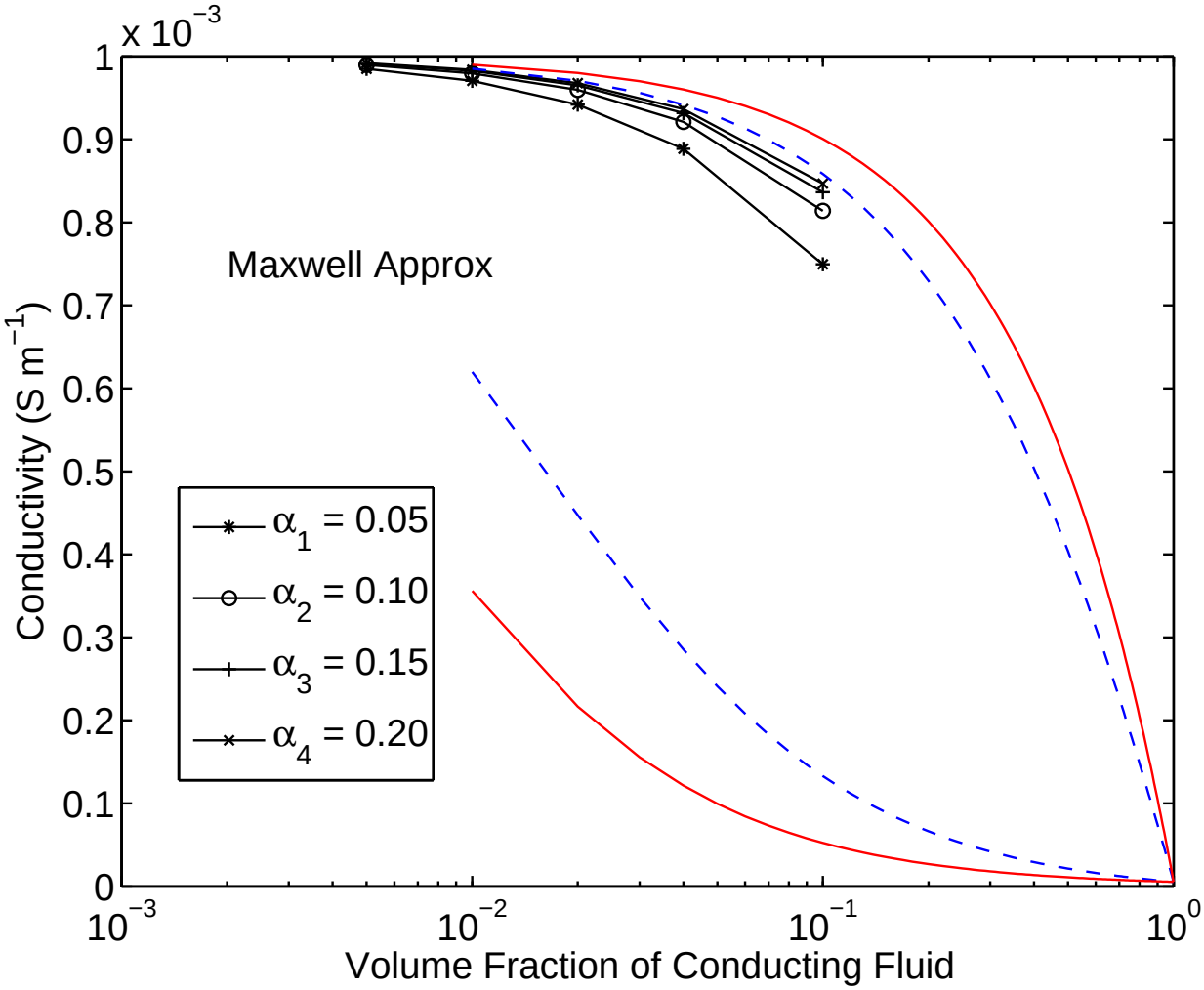

FIG. 5: Log-log plot of effective conductivity estimators for resistive inclusions in a moderately conducting background earth material. Black curves correspond to the Maxwell approximation for four choices of the fracture aspect ratio: $\alpha_1 = 0.05$, $\alpha_2 = 0.10$, $\alpha_3 = 0.15$, and $\alpha_4 = 0.20$. Volume fractions considered are $\phi_2 = 0.005$, 0.01, 0.02, 0.04, and 0.10. Red lines are the upper and lower Wiener bounds on conductivity. The dashed blue lines are the upper and lower Hashin-Shtrikman bounds. The host medium is assumed to be a basalt (or dry sand) having conductivity $\sigma_0 \simeq 0.001$ S$\cdot$ m^{-1}. The resistive fluid inside the fractures is assumed to have conductivity $\sigma_2 \simeq 5.5 \times 10^{-6}$ S$\cdot$ m^{-1}. Note that the smallest aspect ratios result in the largest changes from the host value at a fixed porosity. The biggest effect is clearly for small aspect ratio ($\alpha_1 = 0.05$), from which we infer that these insulating fractures create blockages so that current must flow around these inclusions, thereby causing a very noticeable reduction in overall conductivity.

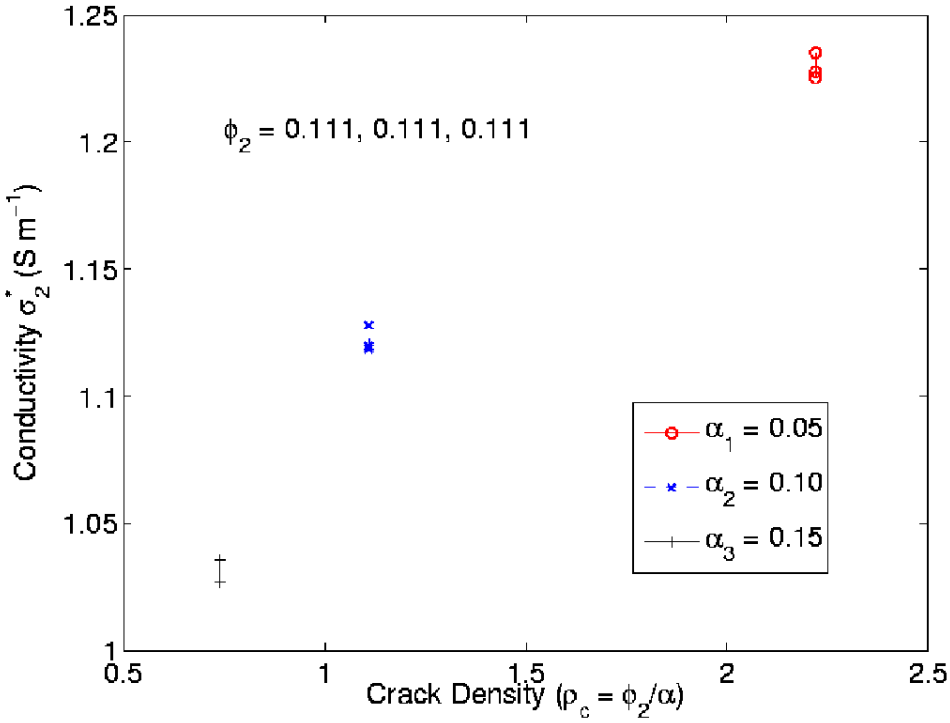

FIG. 6: First of three figures illustrating results obtained using a self-consistent effective medium theory for anisotropic electrically conducting fluid-filled fractures. The model consists of three distinct oriented fracture sets, each of which is imbedded in the same type of host material having low conductivity σ_0, with much higher conductivity material (such as ocean brine) in the fractures. These three sets of fractures can each have different aspect ratio cracks α_1, α_2, and α_3, as well as different volume fractions (or porosities) ϕ_1, ϕ_2, and ϕ_3, respectively. We keep one volume fraction $\phi_2 = 0.111$ fixed, and also maintain the total crack volume fraction $\overline{\phi}_2 \equiv \phi_1 + \phi_2 + \phi_3$ constant, while permitting both ϕ_1 and ϕ_3 to vary. The conductivity shown here is the diagonal component σ_2^* of the resulting anisotropic effective medium model. This Figure illustrates results for fixed ϕ_2, but the three aspect ratios are nevertheless still variable — therefore resulting in nonconstant crack densities. It is especially important to note in this case that, while the values of σ_1^* and σ_3^* are both changing substantially (as will be shown in the following two Figures) because their values of crack density are also changing substantially, while in contrast the values shown here are all remaining very nearly constant. Thus, the crack density – while not a perfect measure of this key behavior of a complicated systems – provides one very good measure of an important variable in these systems. It is key to notice that the overall behavior is very simple in this case, as conductivity is clearly an increasing function of the (very nearly uniquely defined) crack density parameter for each fixed value of crack aspect ratio α.

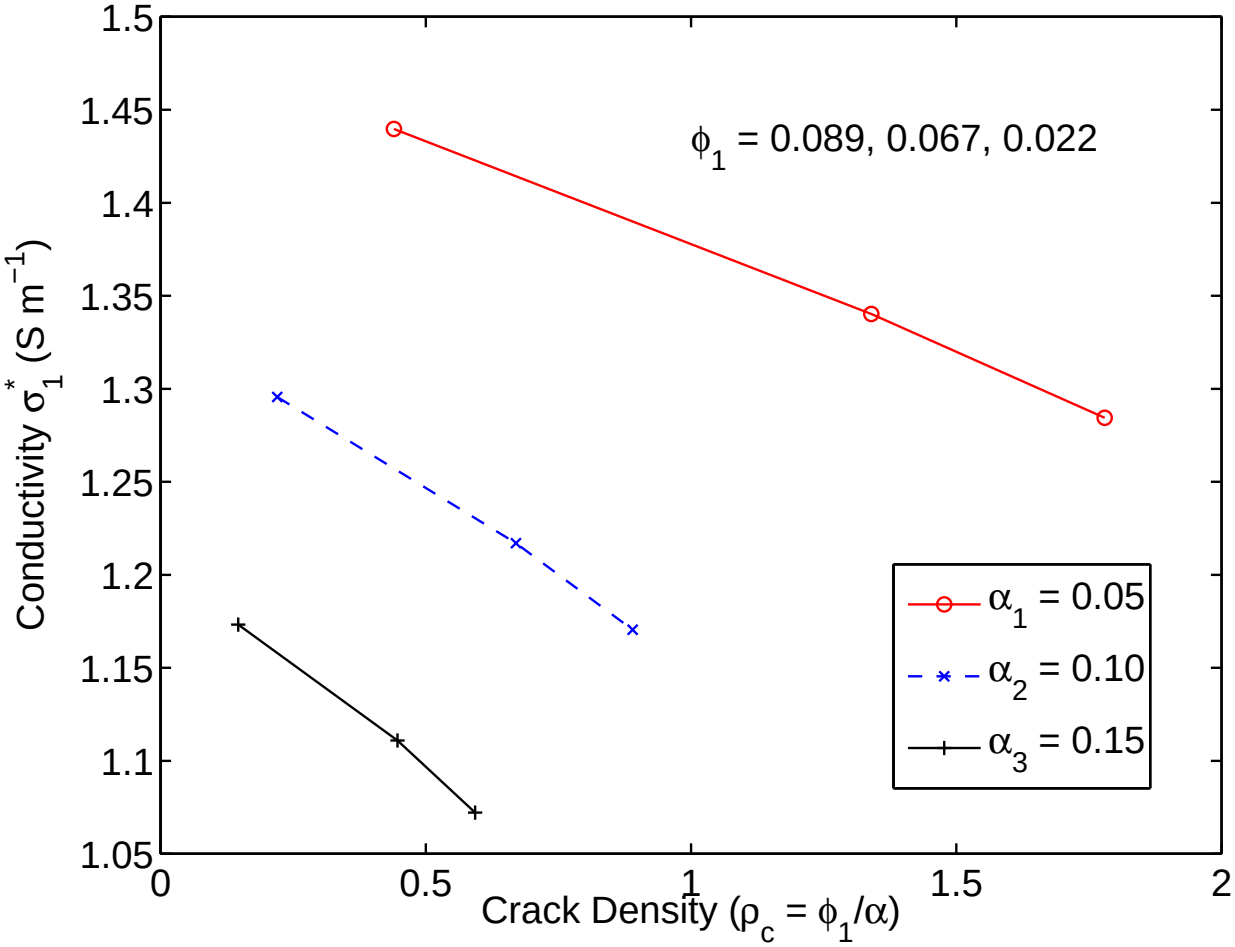

FIG. 7: Second of three figures illustrating results obtained using a self-consistent effective medium theory for anisotropic electrically conducting fluid-filled fractures. The abscissa in each Figure is the crack density $\rho_c \equiv \phi/\alpha$, where α is the aspect ratio of the pertinent cracks, and ϕ is the pertinent porosity. The conductivities shown here are the diagonal components σ_1^* of the anisotropic effective medium model. Thus, this Figure also illustrates (implicitly) results for variable ϕ_1. Conductivity is clearly not a simple increasing function of crack density in this case, as it was in Fig. 6. But for fixed porosity ϕ_1, the conductivity is observed to be a monotonically increasing function of $(1/\alpha)$.

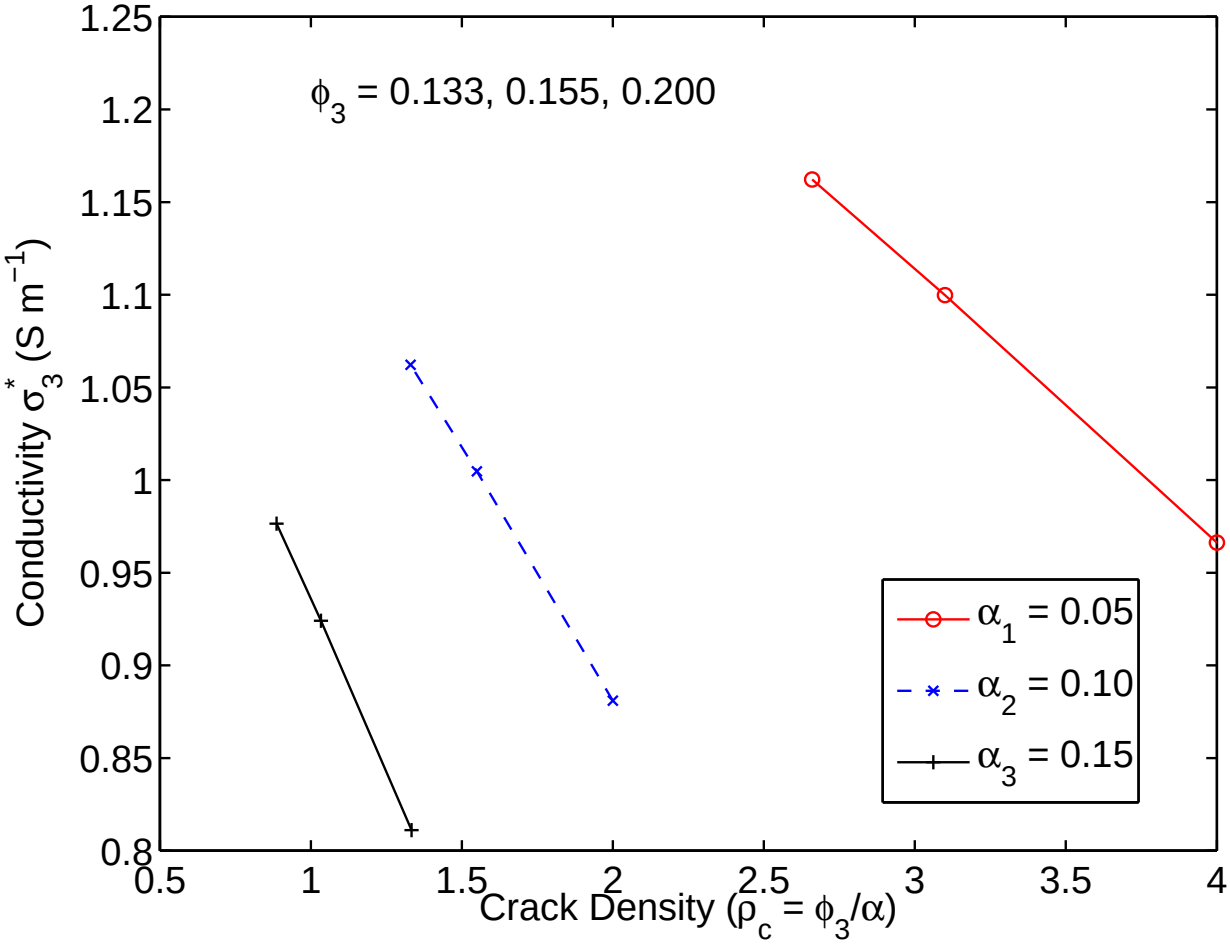

FIG. 8: Third of three figures illustrating results obtained using a self-consistent effective medium theory for anisotropic electrically conducting fluid-filled fractures. The conductivity shown here is the diagonal component σ_3^* of the anisotropic effective medium model. This Figure also illustrates (again implicitly) results for variable ϕ_3. Conductivity is clearly not a simple increasing function of crack density in this case, as it was in Fig. 6. But for fixed porosity ϕ_3, the conductivity is observed to be a monotonically increasing function of $(1/\alpha)$ (as was also true in Fig. 7).

DISCLAIMER

This document was prepared as an account of work sponsored by the United States Government. While this document is believed to contain correct information, neither the United States Government nor any agency thereof, nor The Regents of the University of California, nor any of their employees, makes any warranty, express or implied, or assumes any legal responsibility for the accuracy, completeness, or usefulness of any information, apparatus, product, or process disclosed, or represents that its use would not infringe privately owned rights. Reference herein to any specific commercial product, process, or service by its trade name, trademark, manufacturer, or otherwise, does not necessarily constitute or imply its endorsement, recommendation, or favoring by the United States Government or any agency thereof, or The Regents of the University of California. The views and opinions of authors expressed herein do not necessarily state or reflect those of the United States Government or any agency thereof or The Regents of the University of California.

Ernest Orlando Lawrence Berkeley National Laboratory is an equal opportunity employer.